Relative sea-level response to Little Ice Age ice mass change in south central Alaska: reconciling model predictions and geological evidence

Authors

Natasha Barlow[a]

Ian Shennan[a]

Antony Long[a]

[a] Sea Level Research Unit, Department of Geography, Durham University, South Road, Durham, DH1 3LE, UK

Corresponding author

Natasha Barlow. Email: n.l.m.barlow@durham.ac.uk. Telephone: +44(0) 191 334 1800

Citation

Barlow, N.L.M., Shennan, I. & Long, A.J. Relative sea-level response to Little Ice Age ice mass change in south central Alaska: Reconciling model predictions and geological evidence. *Earth and Planetary Science Letters*. 2012;315-316:62-75.

Abstract

Integration of geological data and glacio-isostatic adjustment (GIA) modelling shows that it is possible to decouple complex mechanisms of relative sea-level (RSL) change in a tectonically active glacial environment. We model a simplest solution in which RSL changes in upper Cook Inlet, Alaska, are a combination of the interplay of tectonic and isostatic processes driven by the unique rheology of this tectonically active location. We calculate interseismic uplift during latter part of the penultimate earthquake cycle to vary from 0.3 to 0.7 mm/yr. Diatom based reconstructions of RSL from tidal marsh sediment sequences coupled with detailed age models, from AD 1400 to the AD 1964 great earthquake, show deviations from a purely tectonically driven model of regional RSL. Glacial isostatic modelling, constrained by GPS data, predicts up to 70 cm sea-level change due to mountain glacier mass balance changes during the Little Ice Age. Misfits between the GIA model predictions and RSL reconstructions in the 19th and 20th century highlight that the tidal marshes of upper Cook Inlet potentially record a hemispheric-wide acceleration in sea level and that other more complex Earth process combinations may contribute to regional RSL change.

1 Introduction

Sediment sequences from the coastal zone of south central Alaska potentially record evidence of two major environmental processes: active tectonics, and the growth and melt of mountain glaciers. Collision between the Pacific oceanic plate and the North American continental plate along the Aleutian megathrust and Yakautat microplate (Figure 1) creates great subduction zone earthquakes, such as the AD 1964 M_w 9.2 Alaska earthquake, and leads to active mountain building close to the coast, reaching over 5400 m above sea level at Mount St Elias. These coastal mountain ranges support the largest glacier systems outside of Antarctica and Greenland (Molnia, 2008) and changes in their mass contribute significantly to global sea-level change. Mass loss following Little Ice Age (LIA) maxima in southern Alaska and British Columbia is estimated to supply over half the contribution to global sea level from sources outside Greenland and Antarctica during the past 50 years, equivalent to 0.12 ± 0.02 mm yr^{-1} from 1962 to 2006 (Berthier et al., 2010). Radic and Regine (2010) predict the melting of Alaskan glaciers may add a further 0.026 ± 0.007 m by AD 2100. Both the advance and retreat of mountain glaciers and tectonic crustal deformation drive local and regional sea-level changes. In this paper we attempt to assess the glacial isostatic adjustment (GIA) and tectonic components of relative sea-level (RSL) change by integrating existing models of the earthquake deformation cycle and LIA ice mass balance in south central Alaska.

Reconstructing past ice volumes requires modelling the GIA process, validated against RSL reconstructions (Milne et al., 2002; Peltier, 2004). Global GIA models estimate, with varying success, post Last Glacial Maximum (LGM) RSL changes recorded along passive coastal margins (examples include: Argus and Peltier, 2010; Bradley et al., 2011; Lambeck, 1995, 2002; Lambeck and Purcell, 2005; Milne et al., 2006; Peltier, 2004). With the plate boundary location of south central Alaska two critical complications arise. First, we cannot use the Earth model parameters from global GIA models such as ICE-5G (VM2) (Peltier, 2004) which are tuned to mid continental and non-tectonic coastline locations, and do not allow for the combined effects of a subducting plate and a low

viscosity zone between the lithosphere and upper mantle. Studies of crustal deformation following great earthquakes along Pacific subduction zones infer the presence of a low viscosity ($<10^{20}$ Pa s) zone (Suito and Hirahara, 1999; Suito et al., 2002; Suito and Freymueller, 2009; Thatcher et al., 1980), termed the asthenosphere, which is fundamental in allowing plate movement (Anderson, 1975). Secondly, vertical land surface deformation during each stage of every earthquake cycle (Figure 2) will combine with glacial isostatic processes to influence RSL.

Regional GIA may be driven by late Holocene mountain glacier mass balance changes. During the last millennium in south central Alaska, mountain glaciers exhibited three phases of glacial advance; ~AD 1180 to 1320, ~AD 1540 to 1710 and ~AD 1810 to 1890, resulting in Holocene maxima for many land-terminating glaciers in the Chugach and Kenai Mountains (Barclay et al., 2009; Calkin et al., 2001; Molnia, 2008; Wiles and Calkin, 1994; Wiles et al., 1999; 2008). These advances occurred during the period termed the Little Ice Age, overlapping with the penultimate great earthquake cycle in south central Alaska, from the penultimate ~AD 1100 great earthquake to the AD 1964 earthquake (Figure 2). We hypothesise that the interplay of GIA and tectonics combines to produce a complex RSL history over the last 1000 years in upper Cook Inlet.

This paper takes a new approach in south central Alaska by combining sea level reconstructions with a regional GIA model and the earthquake deformation cycle (EDC) model. The EDC model summarises the phases of coseismic land uplift or subsidence and the intervening periods of interseismic deformation during cycles of great earthquakes at a particular subduction zone (Figure 2). To date, RSL reconstructions from tidal marshes in south central Alaska largely focus on the sea-level changes associated with the periods of coseismic submergence or uplift (Hamilton and Shennan, 2005a; 2005b; Hamilton et al., 2005; Shennan and Hamilton, 2006; Shennan et al., 2008; 2009; Zong et al., 2003), rather than the RSL changes between earthquakes. Global GIA models do not include spatially and temporally high resolution mountain glacier LIA ice models. In this paper, we apply both GIA modelling and methods of RSL reconstruction with the aim of testing models of

RSL change in south central Alaska from AD 1400 to 1964. This is the part of the LIA for which we have peat-dominated coastal sediments that record RSL change and provide material to create an adequate age model, and avoid the coseismic stages, AD 1964 and ~AD 1100, of the EDC (Figure 2). Our aim is to contribute to knowledge of the EDC in Alaska, and more widely to efforts to quantify the influence of small-scale, recent changes in ice load on RSL. Such knowledge is important as we seek to integrate more closely RSL data from geological timescales with the current geodetic era and for a more complete understanding of modern global sea level changes.

2 Models of the earthquake cycle and glacial isostatic adjustment in south central Alaska

Research in the Pacific North West, Alaska and Japan produces various models of the cycle of land uplift and subsidence during and between great earthquakes through the Holocene (termed earthquake deformation cycles) with each applicable to specific subduction zones (Atwater, 1987; 1992; Atwater et al., 1995; Atwater and Hemphill-Haley, 1997; Hamilton and Shennan, 2005a; Kelsey and Bockheim, 1994; Kelsey et al., 2002; Long and Shennan, 1994; 1998; Nelson et al., 1995; 1996a; 1996b; 2006; Savage and Thatcher, 1992; Sawai, 2001; Shennan et al., 1996; Thatcher, 1984). Using the criteria established by Nelson et al. (1996b) to test for regional co-seismic submergence accompanying a great earthquake and radiocarbon dating in situ horizontally bedded plant macrofossils from the top of fossil peat layers, seven great earthquakes have been identified in the last 4000 years in upper Cook Inlet (Hamilton and Shennan, 2005a; 2005b; Shennan and Hamilton, 2006; Shennan et al., 2008). Similarities between each earthquake cycle leads to an EDC model for upper Cook Inlet with coseismic submergence and RSL rise, followed by rapid post-seismic uplift and RSL fall in the decades after the earthquake (Figure 2). This merges into centuries of slower interseismic uplift before a hypothesised period of pre-seismic subsidence. This pre-seismic phase has not been corroborated outside of upper Cook Inlet. Tidal marshes record the cycles by a series of peat-silt couplets, where a regressive sequence of peat, containing fresh water diatoms accumulates over time due to gradual interseismic land uplift of the continental plate and associated

RSL fall, rapidly subsiding during a great earthquake and overlain by tidal flat sediment containing marine-brackish diatoms (Figure 2).

There are known deviations from the expected EDC model. Within the most recent peat layer, submerged in AD 1964, at Girdwood and Kenai, Hamilton and Shennan (2005a; 2005b) record a decimetre scale RSL rise, followed by a decimetre scale RSL fall which deviates from the proposed four-stage EDC model (Figure 2). They hypothesise this RSL rise-fall oscillation is a consequence of GIA to LIA glacier advance and retreat in the nearby Kenai and Chugach Mountains (Calkin et al., 2001; Wiles and Calkin, 1994; Wiles et al., 2008).

Recent studies support the hypothesis that LIA glacier advance and retreat and the associated surface load changes have the potential to invoke a viscoelastic response in a tectonic location where a thin lithosphere overlies a low viscosity asthenosphere. Along the transform fault of southeast Alaska, mountain and tidewater glaciers have lost 3030 km^3 ice volume from their regional AD 1750 LIA maximum (Larsen et al., 2005). Dendrochronologic records at Juneau show 3.2 m of uplift since ~AD 1780 (Motyka, 2003) and raised shorelines in upper Lynn Canal record 5.7 m in the same period (Larsen et al., 2005). GPS measurements demonstrate continuing rapid uplift of >25 mm yr^{-1} (Larsen et al., 2004). Geological studies in Icy Bay correlate the fluctuating RSL with periods of regional glacier advance and retreat (Mann and Streveler, 2008). Away from Alaska, but along a similarly tectonically active coastal margin, GPS measurements from the Patagonian coast of Chile also record rapid crustal uplift (~39 mm yr^{-1}) likely in response to ice mass loss following the LIA (Dietrich et al., 2010; Rignot et al., 2003). In southeast Alaska, British Columbia and Patagonia, regional late Holocene GIA models require a low viscosity asthenosphere (2.4 to 4.0 x 10^{18} Pa s and 4.0 to 8.0 x 10^{18} Pa s respectively) to fit field observations with model predictions (Dietrich et al., 2010; Ivins and James, 1999; Klemann et al., 2007; Larsen et al., 2005). Modelling GIA displacement at plate boundaries requires regionally specific Earth models with a low viscosity asthenosphere, a

high resolution regional ice load history and short time steps, rather than the typically 0.5-1 k yr time intervals in global post LGM GIA models.

In the next section we outline the methods of RSL reconstruction and GIA modelling that we use to test the hypothesis that GIA RSL overprints tectonically driven land-level changes during the last earthquake cycle.

3 Methods and outcomes of relative sea level reconstruction and glacial isostatic adjustment modelling

3.1 Reconstructing relative sea-level change in upper Cook Inlet, AD 1400 to 1964

Tidal marshes at four sites in upper Cook Inlet provide material for RSL reconstructions along a transect that increases in distance from the LIA centre of ice load within the Chugach Mountains (Figure 1). At Girdwood, closest to the LIA loading centre and the Aleutian trench (~270 km to the south east), we use the original core that led to the hypothesis by Hamilton and Shennan (2005a) that LIA GIA overprints EDC driven RSL, along with a second core to test for within-site variance (cores GW-1 and GW-2b respectively). We use new cores from Bird Point (BP-6), a small marsh west of Girdwood, and Ocean View, OV-4, from the Coral Lane transect previously reported in Hamilton et al. (2005). At Kenai, we use the record from Hamilton and Shennan's (2005b) site 7, labelled here as KE-7. The stratigraphy at all four sites is very similar (supplementary information and Hamilton and Shennan, 2005a; 2005b; Hamilton et al., 2005) with a sharp peat-silt boundary marking the penultimate great earthquake, followed by a regressive sequence (Figure 2) prior to the sharp AD 1964 peat-silt boundary. The only exception is at GW-1 where a ~10 cm silt-peat band interrupts the regressive organic sequence ~12-22 cm from the top of the peat (Hamilton and Shennan, 2005a).

We apply the transfer function methodology and models developed by Hamilton and Shennan (2005a) for reconstructing RSL in upper Cook Inlet. We use an updated modern diatom training set with an additional 16 samples from a previously unsampled tidal marsh at Hope (Figure 1) to improve the range of modern analogues. We follow Hamilton and Shennan (2005a) by calibrating

the fossil diatom assemblages constrained by core lithology. If a sample comes from a fossil peat unit we apply a transfer function model (termed the peat model) based only on those modern diatom samples from above the minimum elevation at which peat accumulates at present. This is ~5 m above mean sea level (MSL), varying slightly as tidal range increases from Kenai towards Turnagain Arm (Figure 4). For a sample from a fossil unit of silt with rootlets, we apply a transfer function with all those samples from ~3 m above MSL (Figure 4), since vegetation starts to colonise the modern tidal flats above this elevation. We develop the transfer functions using the unimodal regression weighted averaging partial least squares (WA-PLS) technique in C2 (version 1.6.8, Juggins, 2003). We tested the transfer function predicted palaeo marsh surface elevation (PMSE) of every fossil peat sample by applying both transfer functions to check for model-dependent outliers and found no over prediction of elevation of samples using the 'peat' training set.

For each fossil diatom assemblages from the base of the peat unit to the top of the peat layer marking the AD 1964 earthquake, the transfer function models produce estimates of PMSE (see supplementary information). Subtracting the PMSE for a given sample (m MHHW) from its core depth (m MHHW) produces estimates of RSL.

3.2 Radiocarbon chronology and age-depth model development

We develop a chronology for three of our cores, GW-2b, BP-6 and KE-7 using AMS radiocarbon samples (Table 1) of either seeds of the same species or herbaceous leaves and stems, along with the upper contact of the main peat layer known to be AD 1964. Dating material from the middle and lower part of the peat layer avoids potential complications with the bomb spike era at the top of the peat layer and possible reworking of material in the underlying tidal silt unit. We produce an age-depth model for the peat layer in each core using the Bayesian *P_sequence* depositional model in OxCal 4.1 (Bronk Ramsey, 1995, 2009) and the IntCal09 calibration curve (Reimer et al., 2009). The *P_sequence* model allows for random variation in sediment accumulation and *a priori* knowledge of the stratigraphic position of a sample, producing 2-sigma calibration probability distributions for

each date in sequence and interpolated modelled ages at specified levels. An agreement index (AI) assesses the model accuracy by checking for inconsistencies between the model and the radiocarbon measurements (Blockley et al., 2008; Bronk Ramsey, 2009) (Table 1).

The model outputs for all three sites show a near linear sediment accretion rate through the interseismic peat layer (Figure 4), so we apply the 0.6 mm yr^{-1} rate from GW-2b to GW-1, for which we only know the AD 1964 boundary at top of the peat (Hamilton and Shennan, 2005a). At OV-4 there is no basal chronological horizon, but a date of 929-1056 yr BP on the underlying peat-silt boundary caused by the penultimate great earthquake (Hamilton et al., 2005), provides a minimum age for the sequence. We assume the onset of peat development at OV-4 occurred at a similar time to that at Bird Point (AD1400), and therefore develop a linear age model with an accumulation rate of ~0.9 mm yr^{-1} from AD 1400 to 1964.

In the discussion (section 4) we show the summary diatom assemblages for each core, plotted according to broad salinity preferences, and the quantitative reconstructions of RSL change against the age-depth models.

3.3 Modelling the Little Ice Age glacial isostatic signal

The majority of Alaskan mountain glaciers have lost mass since the LIA maximum, with nearly every glacier that descends below an elevation of ~1500 m currently thinning and/or retreating (Berthier et al., 2010; Chen et al., 2006; Luthcke et al., 2008; Molnia, 2007; 2008). To model the spatial pattern and magnitude of solid Earth displacement during and following the LIA we use the simple postglacial rebound calculator, TABOO (Spada et al., 2003; Spada, 2003; 2004), previously used in studies of GIA in south east Alaska (Larsen et al., 2005). TABOO uses a layered, non-rotating, incompressible, self-gravitating, Maxwell viscoelastic, spherical symmetric Earth model where the density, shear modulus and Maxwell viscosity of each layer is constant (Spada et al., 2003; Spada, 2003). Rotational feedback causes perturbations to rates of solid Earth and geoid deformation. Mitrovica at al. (2005) show that the present day rates of change driven by perturbations in the

rotation vector in south central Alaska in response to LGM surface loading is in the order of 0.0 – 0.1 mm yr^{-1}. Therefore, the rotational perturbations driven by the magnitude of LIA ice load changes is likely to be near to zero and would have minimal consequence on our GIA outputs. Homogenous flat Earth approximation is sufficient to evaluate the effects of variations in regional ice loads that cover less than 20^{o} of the Earth's surface (Ivins and James, 1999) and is therefore appropriate for the spatial scale of upper Cook Inlet.

For an LIA ice model we use the regional "Neoglacial" ice load model developed by Larsen et al. (2004; 2005), derived by extrapolating back the rate of mid 1950's to mid 1990's ice volume changes of 67 glaciers measured by Arendt et al. (2002) using airborne laser altimetry, to estimate a LIA peak volume in AD 1900. There were three phases of LIA glacier advance in southern Alaska, and the earlier volume changes in the Larsen et al.'s Neoglacial ice model are based on the strength of the middle and early advance and retreat cycles relative to the AD 1900 maximum, using Neoglacial terminal moraine positions to estimate differential ice volumes (Figure 5). These changes are spread over 531 spherical symmetrical disks each of 20 km diameter to estimate LIA ice thickness back 2000 years (Figure 5). We expand the spherical harmonic degrees to degree and order 1024 as per Larsen et al. (2005), where each degree equates to ~19.6 km at 60^{o}N, and therefore allows the Earth model to be sensitive to the 20 km diameter disks and to resolve the effects of small ice load changes. The model which does not allow for decadal fluctuations in tidewater glaciers where periodical surges may result in localised GIA, but, the absence of any surging tidewater glaciers in upper Cook Inlet means this process is likely to have negligible impact in our study area.

Seismic observations from subduction margins identify the presence of an asthenosphere between the lithosphere and upper mantle, with the lithosphere-asthenosphere boundary being fundamental in allowing plate movement (Anderson, 1975). Our Earth model solutions incorporate an asthenosphere (to 220 km depth) below a defined lithosphere and overlying a simple homogenous mantle with a viscosity of 4×10^{20} Pa s, similar to Larsen et al. (2005). We consider a suite of eight

sets of Earth model parameters (Table 2), using two values for effective lithospheric thickness and four values for aesthenosphere viscosity. An effective model lithospheric thickness of 60 km is in line with Larsen et al.'s (2005) model for south east Alaska and James et al.'s (2009) model for Cascadia. The higher effective model lithospheric thickness of 110 km is to take into account the combined lithosphere thickened by the overlapping subduction of the Yakutat and Pacific Plates in south central Alaska (Fuis et al., 2008). A 110 km thickened lithosphere is similar or thicker than proposed for some mid continental locations (Bradley et al., 2011; Peltier, 2004; Shennan et al., 2000), however these models do not include an underlying low viscosity asthenosphere. We consider asthenospheric viscosities up to 4 x 10^{19} Pa s, an upper limit inferred from subduction zone earthquakes (Suito and Hirahara, 1999; Suito et al., 2002; Suito and Freymueller, 2009; Thatcher et al., 1980). Thus, the asthenophere has a model viscosity an order of magnitude lower than the underlying upper mantle. Density and elastic properties of the Earth models follow the seismic Preliminary Reference Earth Model (PREM) (Dziewonski and Anderson, 1981). Initial model runs (data not shown) indicate that with the relatively small ice load changes during the LIA, the upper mantle viscosity makes no difference on the predictions of land displacement, but rather asthenophere viscosity is the primary control on land deformation. This means that LIA driven GIA is likely to be largely independent of any long term GIA movement in the upper mantle (section 3.4).

Comparison of GIA model predictions of present day uplift against GPS measurements of current land motions further constrains the choice of Earth model parameters. For sites within upper Cook Inlet we know that current land motions will include rapid post-seismic uplift following the AD 1964 earthquake (Freymueller et al., 2008; Plafker, 1969). Therefore, we reject any model that predicts present day GIA uplift greater than GPS observed uplift (∑ GIA + Tectonic). For present day post-seismic uplift we use GPS measurements for AD 1992-2007 (Freymueller et al., 2008), with the addition of 0.4 mm yr^{-1} (*Z* translation for 60°N) to the stated vertical GPS values to transform the data to the centre of mass of the solid Earth reference frame (Argus et al., 2010; Blewitt, 2003), which allows direct comparison with the GIA model output. Comparison of the GPS data with the

model predictions allows us to reject two sets of model parameters (Figure 6B). All of the accepted Earth models (Table 2) predict present-day differential uplift across our four sites (Figure 7) and greater amplitude of RSL change at the eastern sites, which are closest to the mountain glaciers and ice caps (Figure 1).

3.4 Estimates of late Quaternary glacial isostatic adjustment

The presence of the large LGM Laurentide and Cordilleran ice sheets causes long wavelength solid Earth displacement due to the horizontal displacement of mantle material and deglacial migration of the forebulge which may overprint short term GIA. TABOO is unable to include the complex nature of the late Quaternary ice sheets as summarised by more sophisticated models, such as ICE-5G (VM2) (Peltier, 2004). As discussed, the Earth structure in VM2 (Peltier, 2002), is likely inappropriate for south central Alaska as it does not include a low viscosity zone between the lithosphere and upper mantle, and James et al. (2000; 2009a; 2009b) show there is potential for the VM2 estimated ongoing solid Earth displacement to be too great in a plate boundary location. However, as the response of the asthenospere to unloading is relatively rapid, any long term GIA due to LGM deglaciation will be a consequence of lateral movement of the higher viscosity upper mantle, and therefore, we use the ICE-5G (VM2) outputs (Peltier, 2004) as maximum constraints on long wavelength post LGM GIA in the upper Cook Inlet. ICE-5G (VM2) solutions indicate upper Cook Inlet locations (Anchorage and Nikiski, near Kenai) are presently subsiding at 0.30 mm yr^{-1} due to migration of the post LGM forebulges, falling from 0.32 mm yr^{-1} 100 years ago. Therefore, any tectonic processes or short term GIA occurring during AD 1400 – 1964 are against a background rate of long term GIA subsidence, likely in the order of 0.40 – 0.30 mm yr^{-1}.

3.5 Calculating rates of late Holocene non-seismic relative sea-level change

Estimates in section 3.4 from ICE-5G (VM2) only account for post LGM GIA. Dates from numerous earthquake cycles allow us to calculate the long term trend in non seismic RSL during the late Holocene which includes all long term viscoelastic effects, regional and global eustasy and local, non

tectonic land level changes. We use published ages from peats at the four field sites (Hamilton and Shennan, 2005b; Hamilton et al., 2005; Shennan and Hamilton, 2006; Shennan et al., 2008; 2010) along with new dates (Table 1) that represent the latter stage of each EDC. Assuming all the strain accumulated during the interseismic period is released coseismically and that negligible permanent deformation occurs over multiple cycles, all four sites show a linear trend in RSL (Figure 8), also seen through multiple cycles in Washington and Oregon (Long and Shennan, 1998).

3.6 Estimating interseismic land motions during the earthquake deformation cycle

To calculate rates of interseismic land movement during the last full earthquake cycle we use the Hamilton and Shennan (2005a) equation which separates the different components of RSL for a complete EDC recorded by a peat-silt couplet within a tidal marsh sediment profile, from one peat-silt boundary to the next, overlying, one:

$$\Delta\xi_{int}(\tau) = \Delta\xi_{rsl}(\tau) + \Delta\xi_{cos}(\tau) - \Delta\xi_{sed}(\tau) - \xi_{peat}(\tau) \quad \text{(Equation 1)}$$

- $\Delta\xi_{int}(\tau)$ represents the postseismic and interseismic uplift (m) between two co-seismic events (Figure 2), in this instance the ~AD 1100 and AD 1964 earthquakes;

- $\Delta\xi_{rsl}(\tau)$ is non-seismic relative sea-level change over the time period in question (including tidal regime changes) (m) calculated using the long term RSL rates in Figure 8;

- $\Delta\xi_{cos}(\tau)$ equals co-seismic subsidence accompanying a subduction zone earthquake (m) estimated by reconstructing the RSL over a peat-silt boundary using the diatom transfer function method outlined in section 3.1;

- $\Delta\xi_{sed}(\tau)$ is net sedimentation (m) (that includes any consolidation, which we are unable to quantify separately) measured in the field from the top of the lower (~AD 1100) peat layer to the top of the upper (AD 1964) peat layer;

- $\xi_{peat}(\tau)$ is the difference (m) in the PMSE of the top of the first buried peat ($\xi_{peat1}(\tau)$) and the PMSE of the top of the second buried peat ($\xi_{peat2}(\tau)$) as reconstructed using the diatom transfer function method outlined in section 3.1.

Solving this equation provides a reconstruction for a complete EDC, in contrast to post-AD 1964 GPS observations (Freymueller et al., 2008) that only deal with a small portion of one cycle and which include a post-seismic land motion term. We can also solve the equation for separate parts of the earthquake cycle if we have ages and PMSE's for intermediate layers within an EDC. Solving the equation for each site in Table 3 shows a significant reduction in the interseismic uplift rate in the latter part of the previous EDC from ~AD 1400 at Girdwood, Bird Point and Ocean View, to 0.74, 0.57 and 0.30 mm yr^{-1} respectively, and highlights a trend of decreasing rates of uplift from Girdwood to Ocean View with distance from the Aleutian trench. This pattern is in line with Sawai et al.'s (2004) model of vertical displacement following a 17th century earthquake along the Kuril subduction zone, Japan, which shows decreasing deep post seismic creep for locations >160 km from the trench. At Kenai the rate is 0.71 mm yr^{-1} but we have no figures for the whole cycle because we have found no sedimentary evidence of the ~AD 1100 earthquake at the site (Hamilton and Shennan, 2005b). These calculations for interseismic uplift provide a template against which to test our RSL reconstructions in section 4.

4 Discussion: reconciling relative sea level reconstructions with glacial isostatic adjustment and earthquake deformation cycle model predictions

To test the hypothesis that LIA GIA solid Earth displacement overprints tectonic land level changes (Figure 2), we compare the RSL reconstructions outlined in section 3.1 and 3.2 from the four sites in upper Cook Inlet with the RSL changes predicted by the EDC model (section 3.6) and test whether the GIA models in section 3.3 can explain any deviations from the EDC model (Figure 9). We use a simple assessment as to the degree of fit between the RSL reconstructions and the models of GIA

and tectonic RSL change by calculating the percentage of diatom based RSL reconstruction data points from each core that overlap with the proposed GIA and EDC models of RSL change (Table 4).

4.1 Relative sea level reconstructions

The summary diatom assemblages for each core (Figure 9A) show changes in the proportion of freshwater to marine and brackish diatoms up core. At GW-1 and GW-2b the percentage of freshwater and salt-intolerant diatoms peak at ~AD 1450-1500 and again at ~AD 1850, between this there is an increase in the proportion of marine-brackish diatoms ~AD 1700 and another increase from AD 1900. The pattern is similar at KE-7 though the freshwater diatoms peaks are later at ~AD 1750 and ~AD 1900 and the marine-brackish proportion increases ~AD 1850 and similarly following AD 1900. At BP-6 and OV-4 there is a general trend of increasing proportion of salt-intolerant diatoms though the proportion of marine-brackish diatoms increases in both cores ~AD 1650 – 1750 relative to the percentages of freshwater diatoms. We convert PMSE estimates for each fossil assemblage (see supplementary information) to changes in RSL in the remainder of Figure 9.

The RSL changes (section 3.1) shown in Figures 9B, 9C and 9D are plotted using the age models from section 3.2. Where summary diatom salinity assemblages show the increase in marine influence the reconstructions show a rise in RSL. Due to the magnitude of the RSL changes quantified by the transfer function models (<50 cm), the changes may fall within sample specific errors, making it hard to quantify the exact magnitude of any RSL change. The large error term of the top three samples in OV-4 reflects a poor fit with the modern diatom samples, and should be treated with the caution suggested by the size of the calculated errors. Mindful of these limitations we test the hypotheses of the drivers of RSL change by plotting the reconstructions over the models of tectonic and GIA RSL changes to assess trends in RSL, rather than try to quantify exact magnitude of change, and therefore assess deviations from the proposed GIA and EDC models.

4.2 Models of glacial isostatic relative sea-level change

Figure 9B shows the RSL reconstructions from the five cores, overlain on the six best Earth model estimates of GIA RSL change associated with the LIA mass balance fluctuations. The modelled RSL takes into account both solid Earth displacement and deformation of the ocean geoid, due to the effects of self-gravitation in the surface mass load (Farrell and Clark, 1976). The curves show RSL rise from ~AD 1500 for all four sites until ~AD 1850, after which RSL begins to fall, with a spatial pattern of decreased RSL change with increased distance from the Chugach Mountains (Figure 7). Many of the RSL reconstructions plot slightly below the modelled RSL, although all at OV-4 overlap with one or more the GIA model RSL curves. By comparison, only 44% and 50% of the reconstructed RSL points from GW-2b and KE-7 respectively achieve fit with a GIA prediction (Table 4). In general the amount of RSL change modelled by TABOO is greater than recorded in the tidal marshes.

Berthier et al. (2010) use digital elevation model (DEM) analysis to suggest ice wastage between AD 1962-2006 is 34% less than estimated by Arendt et al. (2002) and used by Larsen et al. (2005) in their ice model. Therefore, the TABOO modelled LIA RSL change may be up to 34 % greater than actually experienced in upper Cook Inlet, which would result in closer fit with the RSL reconstructions.

4.3 Earthquake deformation cycle modelled relative sea-level change

Figure 9C helps to assess whether the quantitative reconstructions of RSL are solely a consequence of land-level changes associated with the EDC, or whether there is deviation away from the expected model (as summarised in Figure 2). The rates of interseismic land uplift calculated in section 3.6 (Table 3) define the tectonically driven RSL fall from AD 1400 for each site. Our calculations show the interseismic rate declines from Girdwood to Ocean View, with increasing distance from the subduction zone, similar to the pattern of decreasing co-seismic displacement east to west along Turnagain Arm following the AD 1964 earthquake (Plafker, 1969). The exception to the spatial pattern is at Kenai where the estimated interseismic rate is similar to Girdwood. The four GPS sites within 10 km of Kenai record a very high weighted mean 1992-2007 uplift rate of 16.5 ± 1.5 mm/yr

(Figure 6A), with high uplift rates record along much of the south eastern coast of the Kenai Peninsula (Freymueller et al., 2008).

The EDC model includes a hypothesised period of pre-seismic RSL rise prior to the AD 1964 earthquake (Figure 2). There is no consensus as to the existence or timing of any pre-seismic phase of the EDC, however, Karlstrom (1964) notes increased frequency of tidal inundation of Girdwood marsh from AD 1952 and Zong et al (2003) suggest a similar age from ^{137}Cs data. We cannot confirm whether these changes are due to a pre-seismic tectonic process or a 20th century eustastic change. However, to test the complete southern Alaska EDC model (Figure 2) we first include a pre-seismic component in our model of tectonic RSL change. In the absence of any other data we take AD 1952 as the start of the potential pre-seismic RSL rise and calculate a mean rate (15.5 mm yr^{-1}) by averaging the hypothesised pre-seismic rates gained from geological data around upper Cook Inlet (Shennan and Hamilton, 2006, Table 1). Alternatively, the interseismic rate of land uplift may have continued until the AD 1964 co-seismic phase and that there was no pre-seismic RSL rise.

The quantitative RSL reconstructions from all four sites initially follow the pattern of tectonically driven land-level change with an initial RSL fall up to ~AD 1500. However, the RSL reconstructions then deviate from the expected EDC model with a RSL rise, similar to the hypothesised deviations in Figure 2, and coinciding with the middle LIA advance. The reconstructions all consistently plot below the EDC model with maximum fit of 54% between the EDC model and the OV-4 reconstructed data points and minimum fit of only 20% with the GW-1 reconstructions (Table 4). This indicates that the upper Cook Inlet did not continue to experience the magnitude of RSL fall due to interseismic uplift as predicted by the EDC model.

4.4 Combining relative sea level reconstructions and models of relative sea-level change

By adding the GIA model rates in Figure 9B with the EDC model rates of RSL change in Figure 9C produces an estimate of RSL change driven by tectonic land-level deformation, gravitational deformation of ocean geoid and glacial-isostatic solid Earth displacement (Figure 9D). All of the RSL

reconstructed fossil samples of BP-6, OV-4 and KE-7 fit one or more of the combined EDC plus GIA model solutions, and 80% and 89% from GW-1 and GW-2b respectively (Table 4). An exception to the trend is the outlier at ~AD 1625 in GW-2b. This single sample may be a consequence of ice rafting of sediment onto the paleo marsh surface, a process observed on the contemporary marsh (Hamilton et al., 2005). The overlap between model solutions and data values, within both the errors of the RSL reconstructions and spread of GIA model solutions, suggests the simplest hypothesis for the RSL changes experienced in upper Cook Inlet from AD 1400 to 1964 is due to the interplay between short term GIA and interseismic land uplift.

The misfit with the Girdwood data points and the model solutions is due to a reconstructed trend of RSL rise from ~AD 1800 to AD 1964, compared to the GIA model predictions of high sea level at ~AD 1850 as the asthenosphere responds to the late LIA advance from AD 1800, followed by a fall as the glaciers retreat from AD 1900 (Figure 9D). At this stage we cannot say whether this misfit is an artefact of a model input parameter. The ice model assumes a synchronous advance and retreat history for all mountain glaciers which is probably unrealistic. Secondly, the misfit could be a consequence of the linear sediment accumulation model extrapolated to the top of the Girdwood profile, particularly in GW-1 where a layer of silty-peat punctuates the regressive pre-AD 1964 peat layer (section 3.1). However, our radiocarbon dates do not produce good fit with the AD 1952 ^{137}Cs ages associated with the onset of nuclear weapons testing reported by Zong et al. (2003) which suggest a much faster accumulation rate at the top of the Girdwood peat compared to our age-depth models. ^{137}Cs preferentially binds to ions on clays and fine silts and may be remobilised with the decomposition of organics, accelerated by a lowering of the water table (Cooper et al., 1995; Davis et al., 1984), which occurs following co-seismic submergence, potentially mobilising the ^{137}Cs profiles downwards and producing an artificially high estimates of sediment accumulation. If we reject the Zong et al. (2003) hypothesis of a period of rapid pre-seismic sediment accumulation or RSL rise in the decade prior to the AD 1964 earthquake, we should consider a climate origin for sea-level rise. There are numerous estimates of the timing and magnitude of sea level accelerations in

the late 19th to early 20th centuries from tide gauges, geological and geodetic data, and modelling results which vary from ~1.0 to 2.5 mm yr^{-1} (Donnelly et al., 2004; Gehrels et al., 2006; 2008; Holgate and Woodworth, 2004; Kemp et al., 2009; Woodworth et al., 2009a; 2009b). Without further information we are cannot further resolve the cause of the misfit for Girdwood in figure 9D.

Apart from this exception, there is a good level of agreement (Table 4) between the salt marsh reconstructions and models of sea-level change (Figure 9D). Both the reconstructions and model predictions have inbuilt assumptions and errors, and the nature of RSL change means a number of complex, interacting factors control RSL at a given place in space in time. By combining different drivers of sea level we suggest the reconstructed RSL changes in upper Cook Inlet from AD 1400 - 1964 are likely a consequence of LIA GIA, interseismic land uplift, deformation of the ocean geoid and potentially eustatic changes. This all occurs against a background long term rate of RSL change and solid Earth deformation due to the movement of the upper mantle following LGM deglaciation. We do not suggest it is possible to simply separate all these components without error and our results do not preclude other combinations, however we apply Occam's razor, allowing the simplest explanation to exist until refuted. Further testing of the sea level hypotheses and disentangling the mechanisms in Alaska requires integrated GIA and tectonic models, with a regional specific mantle profile and both long and short term ice loads and additional far-field records of recent RSL accelerations.

5 Conclusions

Integration of geological data and GIA modelling shows that it is possible test hypotheses of the different mechanisms of RSL change in a tectonically active glacial environment. As on all coastlines, different processes interact to make it complex to identify the relative importance of individual mechanisms. Using records of RSL change from AD 1400 to 1964 from four sites in upper Cook Inlet we test the hypothesis initially put forward by Hamilton and Shennan (2005a) that GIA during the LIA overprints EDC RSL change. We derive quantitative estimates of the rates of interseismic uplift

during the penultimate EDC cycle and test for deviations from the expected EDC model of RSL change. GIA models of RSL due to solid Earth displacement and deformation of the ocean geoid in association with LIA mountain glacier mass balance changes within south central Alaska estimate up to 70 cm of GIA RSL change during the LIA. In testing the hypothesis that RSL changes in upper Cook Inlet are likely in part due to a combination of the complex interplay of tectonic and isostatic processes driven by the unique rheology of this tectonically active location, we provide one solution within the errors of our RSL reconstructions and GIA model to explain the reconstructed RSL changes, though are mindful that other more complex Earth process combinations may exist. Misfits between the GIA model predictions and RSL reconstructions in the 19th and 20th century highlight that the tidal marshes of upper Cook Inlet potentially record a hemispheric wide acceleration in sea level.

Acknowledgements

Barlow thanks The Royal Society Dudley Stamp Memorial Fund, The Royal Geographical Society Monica Cole Research Grant and Department of Geography, Durham University for financial fieldwork support. Rod Combellick, Smiley Shields, Sarah Grey, Jack Allen and Frank Davies provided assistance in the field. Chugach National Forest allowed access to Bird Point. We thank Chris Larsen for supplying his Alaska Neoglacial ice model. Part of this work was supported by COST Action ES0701 "Improved constraints on models of Glacial Isostatic Adjustment" and by the U.S. Geological Survey, Department of the Interior, under USGS award number #G09AP00105 (The views and conclusions contained in this document are those of the authors and should not be interpreted as necessarily representing the official policies, either expressed or implied, of the U.S. Government). Radiocarbon support was provided by the Natural Environment Research Council Radiocarbon Facility (grants #935.0901 and #1339.1008). This work has benefited greatly from discussions with Sarah Woodroffe, Pippa Whitehouse, Robin Edwards, Matt King and Giorgio Spada, and laboratory assistance from Frank Davies, Neil Tunstall, Martin West, Amanda Hayton and Kathryn Melvin. We thank two anonymous reviewers whose very detailed comments greatly improved this manuscript. This work forms a contribution to PALSEA and IGCP Project 588 "Preparing for Coastal Change".

References

Anderson, D.L., 1975. Accelerated Plate Tectonics. Science 187, 1077-1079.

Ardent, A., Echelmeyer, K., Harrison, W., Lingle, C., Valentine, V., 2002. Rapid wastage of Alaska glaciers and their contribution to rising sea levels. Science 297, 382-386.

Argus, D.F., Gordon, R.G., Heflin, M.B., Ma, C., Eanes, R.J., Willis, P., Peltier, W.R., Owen, S.E., 2010. The angular velocities of the plates and the velocity of Earth's centre from space geodesy. Geophysical Journal International 180, 913-960.

Argus, D.F., Peltier, W.R., 2010. Constraining models of postglacial rebound using space geodesy: a detailed assessment of model ICE-5G (VM2) and its relatives. Geophysical Journal International 181, 697-723.

Atwater, B.F., 1987. Evidence for great Holocene earthquakes along the outer coast of Washington State. Science 236, 942-944.

Atwater, B.F., 1992. Geologic evidence for earthquakes during the past 2000 years along the Copalis River, Southern coastal Washington. Journal of Geophysical Research 97, 1901-1919.

Atwater, B.F., Hemphill-Haley, E., 1997. Recurrence intervals for great earthquakes of the past 3,500 years at northeastern Willapa Bay, Washington. U.S. Geological Survey Professional Paper 1576, 1-108.

Atwater, B.F., Nelson, A.R., Clague, J.J., Carver, G.A., Yamaguchi, D.K., Bobrowski, P.T., Borgeois, J., Darienzo, M.E., Grant, W.C., Hemphill-Haley, E., Kelsey, H.M., Jacoby, G.C., Nishenko, S.P., Palmer, S.P., Peterson, C.D., Reinhart, M.A., 1995. Summary of coastal geologic evidence for past great earthquakes at the Cascadia subduction zone. Earthquake Spectra 11, 1-18.

Barclay, D.J., Wiles, G.C., Calkin, P.E., 2009. Holocene glacier fluctations in Alaska. Quaternary Science Reviews 28, 2034-2048.

Berthier, E., Schiefer, E., Clarke, G.K.C., Menounos, B., Remy, F., 2010. Contribution of Alaskan glaciers to sea-level rise derived from satellite imagery. Nature Geoscience 3, 92-95.

Blewitt, G., 2003. Self-consistency in reference frames, geocenter definition, and surface loading of the solid Earth. Journal of Geophysical Research-Solid Earth 108, 10.

Blockley, S.P.E., Bronk Ramsey, C., Lane, C.S., Lotter, A.F., 2008. Improved age modelling approaches as exemplified by the revised chronology for the Central European varved lake Soppensee. Quaternary Science Reviews 27, 61-71.

Bradley, S.L., Milne, G.A., Shennan, I., Edwards, R., 2011. An improved glacial isostatic adjustment model for the British Isles. Journal of Quaternary Science 26, 541-552.

Bronk Ramsey, C., 1995. Radiocarbon calibration and analysis of stratigraphy: The OxCal program. Radiocarbon 37, 425-430.

Bronk Ramsey, C., 2009. Bayesian Analysis of Radiocarbon Dates. Radiocarbon 51, 337-360.

Calkin, P.E., Wiles, G.C., Barclay, D.J., 2001. Holocene coastal glaciation of Alaska. Quaternary Science Reviews 20, 449-461.

Chen, J.L., Tapley, B.D., Wilson, C.R., 2006. Alaskan mountain glacial melting observed by satellite gravimetry. Earth and Planetary Science Letters 248, 368-378.

Cooper, L.W., Grebmeier, J.M., Larsen, I.L., Solis, C., Olsen, C.R., 1995. Evidence for the re-distribution of Cs-137 in Alaskan tundra, lake and marine sediments. Science of the Total Environment 161, 295-306.

Davis, R.B., Hess, C.T., Norton, S.A., Hanson, D.W., Hoagland, K.D., Anderson, D.S., 1984. Cs-137 and Pb-210 dating of sediments from soft-water lakes in New England (USA) and Scandinavia, a failure of Cs-137 dating. Chemical Geology 44, 151-185.

Dietrich, R., Ivins, E.R., Casassa, G., Lange, H., Wendt, J., Fritsche, M., 2010. Rapid crustal uplift in Patagonia due to enhanced ice loss. Earth and Planetary Science Letters 289, 22-29.

Donnelly, J.P., Cleary, P., Newby, P., Ettinger, R., 2004. Coupling instrumental and geological records of sea-level change: Evidence from southern New England of an increase in the rate of sea-level rise in the late 19th century. Geophysical Research Letters 31.

Dziewonski, A.M., Anderson, D.L., 1981. Preliminary Reference Earth Model. Physics of The Earth and Planetary Interiors 25, 297-356.
Farrell, W.E., Clark, J.A., 1976. On postglacial sea level. Geophysical Journal of the Royal Astronomical Society 46, 647-667.
Freymueller, J.T., Woodard, H., Cohen, S.C., Cross, R., Elliot, J., Larsen, C.F., Hreinsdottir, S., Zweek, C., 2008. Active Deformation Processes in Alaska, based on 15 Years of GPS Measurements, in: Freymueller, J.T., Haeussler, P.J., Wesson, R.L., Ekstrom, G. (Eds.), Active Tectonics and Seismic Potential of Alaska. AGU Geophysical Monograph 179, Washington, DC.
Fuis, G.S., Moore, T.E., Plafker, G., Brocher, T.M., Fisher, M.A., Mooney, W.D., Nokleberg, W.J., Page, R.A., Beaudoin, B.C., Christensen, N.I., Levander, A.R., Lutter, W.J., Saltus, R.W., Ruppert, N.A., 2008. Trans-Alaska Crustal Transect and continental evolution involving subduction underplating and synchronous foreland thrusting. Geology 36, 267-270.
Gehrels, W.R., Hayward, B., Newnham, R.M., Southall, K.E., 2008. A 20th century acceleration of sea-level rise in New Zealand. Geophysical Research Letters 35.
Gehrels, W.R., Marshall, W.A., Gehrels, M.J., Larsen, G., Kirby, J.R., Eiriksson, J., Heinemeier, J., Shimmield, T., 2006. Rapid sea-level rise in the North Atlantic Ocean since the first half of the nineteenth century. Holocene 16, 949-965.
Hamilton, S., Shennan, I., 2005a. Late Holocene relative sea-level changes and the earthquake deformation cycle around upper Cook Inlet, Alaska. Quaternary Science Reviews 24, 1479-1498.
Hamilton, S., Shennan, I., Combellick, R., Mulholland, J., Noble, C., 2005. Evidence for two great earthquakes at Anchorage, Alaska and implications for multiple great earthquakes through the Holocene. Quaternary Science Reviews 24, 2050-2068.
Hamilton, S.L., Shennan, I., 2005b. Late Holocene great earthquakes and relative sea-level change at Kenai, southern Alaska. Journal of Quaternary Science 20, 95-111.
Holgate, S.J., Woodworth, P.L., 2004. Evidence for enhanced coastal sea level rise during the 1990s. Geophysical Research Letters 31, 4.
Ivins, E.R., James, T.S., 1999. Simple models for late Holocene and present-day Patagonian glacier fluctuations and predictions of a geodetically detectable isostatic response. Geophysical Journal International 138, 601-624.
James, T., Gowan, E.J., Hutchinson, I., Clague, J.J., Barrie, J.V., Conway, K.W., 2009a. Sea-level change and paleogeographic reconstructions, southern Vancouver Island, British Columbia, Canada. Quaternary Science Reviews 28, 1200-1216.
James, T.S., Clague, J.J., Wang, K., Hutchinson, I., 2000. Postglacial rebound at the northern Cascadia subduction zone. Quaternary Science Reviews 19, 1527-1541.
James, T.S., Gowan, E.J., Wada, I., Wang, K., 2009b. Viscosity of the asthenosphere from glacial isostatic adjustment and subduction dynamics at the northern Cascadia subduction zone, British Columbia, Canada. Journal of Geophysical Research 114, B04405.
Juggins, S., 2003. C2: A Microsoft Windows program for developing and applying palaeoecological transfer functions and for visualising multi-proxy stratigraphic datasets, 1.4.2 ed. University of Newcastle, Newcastle upon Tyne.
Karlstrom, T.N.V., 1964. Quaternary geology of the Kenai lowland and the glacial history of the Cook Inlet region, Alaska. US Geological Survey Professional Paper 443, 1-69.
Kelsey, H.M., Bockheim, J.G., 1994. Coastal landscape evolution as a function of eustasy and surface uplift rate, Cascadia margin, southern Oregon. Bulletin of the Geological Society of America 106, 840-854.
Kelsey, H.M., Witter, R.C., Hemphill-Haley, E., 2002. Plate-boundary earthquakes and tsunamis of the past 5500 years, Sixes River estuary, southern Oregon. Bulletin of the Geological Society of America 114, 298-314.
Kemp, A.C., Horton, B.P., Culver, S.J., Corbett, D.R., van de Plassche, O., Gehrels, W.R., Douglas, B.C., Parnell, A.C., 2009. Timing and magnitude of recent accelerated sea-level rise (North Carolina, United States). Geology 37, 1035-1038.

Klemann, V., Ivins, E.R., Martinec, Z., Wolf, D., 2007. Models of active glacial isostasy roofing warm subduction: Case of the South Patagonian Ice Field. Journal of Geophysical Research-Solid Earth 112.
Lambeck, K., 1995. Late Devensian and Holocene shorelines of the British Isles and North Sea from models of glacio-hydro-isostatic rebound. Journal of the Geological Society of London 152, 437-448.
Lambeck, K., 2002. Sea Level Change from Mid Holocene to Recent Time: An Australian Example with Global Implications, in: Mitrovica, J.X., Vermeersen, B. (Eds.), Ice Sheets, Sea Level and the Dynamic Earth. AGU Geodynamics Series 29, Washington, DC, pp. 33-50.
Lambeck, K., Purcell, A., 2005. Sea-level change in the Mediterranean Sea since the LGM: model predictions for tectonically stable areas. Quaternary Science Reviews 24, 1969.
Larsen, C.F., Motyka, R.J., Freymueller, J.T., Echelmeyer, K.A., Ivins, E.R., 2004. Rapid uplift of southern Alaska caused by recent ice loss. Geophysical Journal International 158, 1118-1133.
Larsen, C.F., Motyka, R.J., Freymueller, J.T., Echelmeyer, K.A., Ivins, E.R., 2005. Rapid viscoelastic uplift in southeast Alaska caused by post-Little Ice Age glacial retreat. Earth And Planetary Science Letters 237, 548-560.
Long, A.J., Shennan, I., 1994. Sea level changes in Washington and Oregon and the "Earthquake deformation cycle". Journal of Coastal Research 10, 825-838.
Long, A.J., Shennan, I., 1998. Models of rapid relative sea-level change in Washington and Oregon, USA. Holocene 8, 129-142.
Luthcke, S.B., Arendt, A.A., Rowlands, D.D., McCarthy, J.J., Larsen, C.F., 2008. Recent glacier mass changes in the Gulf of Alaska region from GRACE mascon solutions. Journal of Glaciology 54, 767-777.
Mann, D.H., Streveler, G.P., 2008. Post-glacial relative sea level, isostasy, and glacial history in Icy Strait, Southeast Alaska, USA. Quaternary Research 69, 201-216.
Milne, G., Shennan, I., B.A.R., Y., Waugh, A.I., Teferle, F.N., Bingley, R.M., Bassett, S.E., Cuthbert-Brown, C., Bradley, S.L., 2006. Modelling the glacial isostatic adjustment of the UK region. Philosophical Transactions of the Royal Society A - Mathematical Physical and Engineering Sciences 364, 931-948.
Milne, G.A., Mitrovica, J.X., Schrag, D.P., 2002. Estimating past continental ice volume from sea-level data. Quaternary Science Reviews 21, 361-376.
Mitrovica, J.X., Wahr, J., Matsuyama, I., Paulson, A., 2005. The rotational stability of an ice-age earth. Geophysical Journal International 161, 491-506.
Molnia, B.F., 2007. Late nineteenth to early twenty-first century behaviour of Alaskan glaciers as indicators of changing regional climate. Global and Planetary Change 56, 23-56.
Molnia, B.F., 2008. Glaciers of North America - Glaciers of Alaska, in: Williams, R.S., Jr., Ferrigno, J.G. (Eds.), Satellite images atlas of glaciers of the world. US Geological Survey Professional Paper 1386-K p525.
Motyka, R.J., 2003. Little Ice Age subsidence and post Little Ice Age uplift at Juneau, Alaska, inferred from dendrochronolgy and geomorphology. Quaternary Research 59, 300-309.
Nelson, A.R., Atwater , B.F., Bobrowski, P.T., Bradley, L.A., Clague, J.J., Carver, G.A., Darienzo, M.E., Grant, W.C., Krueger, H.W., Sparks, R., Stafford, T.W.J., Stuvier, M., 1995. Radiocarbon evidence for extensive plate-boundary rupture about 300 years ago at the Cascadia subduction zone. Nature 378, 371-374.
Nelson, A.R., Jennings, A.E., Kashima, K., 1996a. An earthquake history derived from stratigraphic and microfossil evidence of relative sea-level change at Coos Bay, southern coastal Oregon. Geological Society of America Bulletin 108, 141-154.
Nelson, A.R., Kelsey, H.M., Witter, R.C., 2006. Great earthquakes of variable magnitude at the Cascadia subduction zone. Quaternary Research 65, 354-365.
Nelson, A.R., Shennan, I., Long, A.J., 1996b. Identifying coseismic subsidence in tidal-wetland stratigraphic sequences at the Cascadia subduction zone of western North America. Journal Of Geophysical Research-Solid Earth 101, 6115-6135.

Peltier, W.R., 2002. Global glacial isostatic adjustment: palaeogeodetic and space geodetic test of the ICE-4G (VM2) model. Journal of Quaternary Science 17, 491-510.
Peltier, W.R., 2004. Global glacial isostasy and the surface of the ice-age earth: The ICE-5G (VM2) model and GRACE. Annual Review of Earth and Planetary Sciences 32, 111-149.
Plafker, G., 1969. Tectonics of the March 27, 1964, Alaska earthquake. U.S. Geological Survey Professional Paper 543-I, 74.
Reimer, P.J., Baillie, M.G.L., Bard, E., Bayliss, A., Beck, J.W., Blackwell, P.G., Ramsey, C.B., Buck, C.E., Burr, G.S., Edwards, R.L., Friedrich, M., Grootes, P.M., Guilderson, T.P., Hajdas, I., Heaton, T.J., Hogg, A.G., Hughen, K.A., Kaiser, K.F., Kromer, B., McCormac, F.G., Manning, S.W., Reimer, R.W., Richards, D.A., Southon, J.R., Talamo, S., Turney, C.S.M., van der Plicht, J., Weyhenmeye, C.E., 2009. IntCal09 and Marine09 radiocarbon age calibration curves, 0-50,000 years cal BP. Radiocarbon 51, 1111-1150.
Rignot, E., Rivera, A., Casassa, G., 2003. Contribution of the Patagonia Icefields of South America to sea level rise. Science 302, 434-437.
Savage, J.C., Thatcher, W., 1992. Interseismic deformation at the Nankai Trough, Japan subdcution zone. Journal of Geophysical Research 97, 11,117-111,135.
Sawai, Y., 2001. Episodic emergence in the past 3000 years at the Akkeshi estuary, Hokkaido, northern Japan. Quaternary Research 56, 231-241.
Sawai, Y., Satake, K., Kamataki, T., Nasu, H., Shishikura, M., Atwater, B.F., Horton, B.P., Kelsey, H.M., Nagumo, T., Yamaguchi, M., 2004. Transient uplift after a 17th-Century earthquake along the Kuril subduction zone. Science 306, 1918-1920.
Shennan, I., Barlow, N., Combellick, R., 2008. Palaeoseismological records of multiple great earthquakes in south-central Alaska: a 4000 year record at Girdwood, in: Freymueller, J.T., Haeussler, P.J., Wesson, R.L., Ekstrom, G. (Eds.), Active tectonics and seismic potential of Alaska. AGU Geophysical Monograph Series Vol 179, Washington, DC, pp. 185-199.
Shennan, I., Bruhn, R., Plafker, G., 2009. Multi-segment earthquakes and tsunami potential of the Aleutian megathrust. Quaternary Science Reviews 28, 7-13.
Shennan, I., Hamilton, S., 2006. Coseismic and pre-seismic subsidence associated with great earthquakes in Alaska. Quaternary Science Reviews 25, 1-8.
Shennan, I., Lambeck, K., Horton, B., Innes, J., Lloyd, J., McArthur, J., Purcell, T., Rutherford, M., 2000. Late Devensian and Holocene records of relative sea-level changes in northwest Scotland and their implications for glacio-hydro-isostatic modelling. Quaternary Science Reviews 19, 1103-1135.
Shennan, I., Long, A., Barlow, N., Watcham, E., 2010. Spatial and Temporal Patterns of Deformation Associated with Multiple Late Holocene Earthquakes in Alaska. USGS/NEHRP Final Technical Report. (External Grant Award # G09AP00105).
Shennan, I., Long, A.J., Rutherford, M.M., Green, F.M., Innes, J.B., Lloyd, J.M., Zong, Y., Walker, K.J., 1996. Tidal marsh stratigraphy, sea-level change and large earthquakes, I: A 5000 year record in Washington, USA. Quaternary Science Reviews 15, 1023-1059.
Spada, G., 2003. The Theory Behind TABOO. Samizdat Press, Golden-White River Junction.
Spada, G., Antonioli, A., Boschi, L., Brandi, V., Cianetti, S., Galvani, G., Giunchi, C., Perniola, B., Piana Agostinetti, N., Piersanti, A., Stocchi, P., 2003. TABOO, User Guide. Samizdat Press, Golden-White River Junction.
Spada, G., Antonioli, A., Boschi, L., Brandi, V., Cianetti, S., Galvani, G., Giunchi, C., Perniola, B., Piana Agostinetti, N., Piersanti, A., Stocchi, P., 2004. Geodesy: modeling earth's post-glacial rebound. Eos Transactions. AGU 85, 62.
Suito, H., Freymueller, J.T., 2009. A viscoelastic and afterslip postseismic deformation model for the 1964 Alaska earthquake. Journal of Geophysical Research-Solid Earth 114.
Suito, H., Hirahara, K., 1999. Simulation of Postseismic Deformations caused by the 1896 Riku-u Earthquake, Northeast Japan: Re-evaluation of the viscosity in the upper mantle. Geophysical Research Letters 26, 2561-2564.
Suito, H., Iizuka, M., Hirahara, K., 2002. 3-D viscoelastic FEM Modeling of crustal deformation in northeast Japan. Pure and Applied Geophysics 159, 2239-2259.

Thatcher, W., 1984. The earthquake deformation cycle at the Nankai Trough, Southwest Japan. Journal of Geophysical Research 89, 3087-3101.
Thatcher, W., Matsuda, T., Kato, T., Rundle, J.B., 1980. Lithospheric Loading by the 1896 Riku-U Earthquake, Northern Japan - Implications for Plate Flexure and Asthenospheric Rheology. Journal of Geophysical Research 85, 6429-6435.
Wiles, G.C., Barclay, D.J., Calkin, P.E., 1999. Tree-ring-dated 'Little ice age' histories of maritime glaciers from western Prince William Sound, Alaska. Holocene 9, 163-173.
Wiles, G.C., Barclay, D.J., Calkin, P.E., Lowell, T.V., 2008. Century to millennial-scale temperature variations for the last two thousand years indicated from glacial geologic records of southern Alaska. Global and Planetary Change 60, 115-125.
Wiles, G.C., Calkin, P.E., 1994. Late Holocene, high resolution glacial chronologies and climate, Kenai mountains, Alaska. Geological Society of America Bulletin 106, 281-303.
Woodworth, P., Teferle, F., Bingley, R., Shennan, I., Williams, S., 2009a. Trends in UK mean sea level revisited. Geophysical Journal International 176, 19-30.
Woodworth, P.L., White, N.J., Jevrejeva, S., Holgate, S.J., Church, J.A., Gehrels, W.R., 2009b. Evidence for the accelerations of sea level on multi-decade and century timescales. Int. J. Climatol. 29, 777-789.
Zong, Y., Shennan, I., Combellick, R.A., Hamilton, S.L., Rutherford, M.M., 2003. Microfossil evidence for land movements associated with the AD 1964 Alaska earthquake. Holocene 13, 7-20.

Lab code	Sample code	Depth (cm)	14C yr BP (± 1σ)	Calibrated age (2σ yr AD)		*P_sequence* modelled calibrated age(2σ yr AD)		Agreement index
				Minimum	Maximum	Minimum	Maximum	
Girdwood (GW-2b)								$A_{overall}$ = 80.4
SUERC-31174	GW-2b-R1	60	272 ± 37	1489	1953	1773	1803	*57**
SUERC-31175	GW-2b-R2	64	116 ± 35	1678	1940	1692	1749	101
SUERC-31176	GW-2b-R5	76	374 ± 37	1444	1635	1493	1569	72
SUERC-31177	GW-2b-R6	80	433 ± 37	1414	1619	1440	1498	96
SUERC-31178	GW-2b-R7	84	537 ± 37	1310	1442	1391	1436	128
SUERC-31179	GW-2b-R8	88	620 ± 37	1289	1404	1333	1385	109
SUERC-31180	GW-2b-R9	92	629 ± 35	1287	1400	1280	1328	98
Bird Point (BP-6)								$A_{overall}$ = 83.6
SUERC-22662	BP-6-R1	76	110 ± 37	1679	1940	1803	1855	112
SUERC-22666	BP-6-R3	84	125 ± 37	1675	1942	1686	1743	104
SUERC-22667	BP-6-R4	88	250 ± 37	1516	1955	1635	1685	125
SUERC-22668	BP-6-R5	92	248 ± 37	1517	1955	1579	1645	*24**
SUERC-22669	BP-6-R7	100	368 ± 35	1447	1635	1477	1536	108
SUERC-22670	BP-6-R8	104	399 ± 37	1435	1632	1435	1485	138
SUERC-22671	BP-6-R9	108	549 ± 37	1306	1438	1384	1435	119
Kenai (KE-7)								$A_{overall}$ = 95.7
AA-50484	KE-7-R1	9	31 ± 51	1682	1933	1814	1906	92
AA-50485	KE-7-R2	13	71 ± 28	1691	1920	1689	1834	91
CAMS-93963†	KE-7-R3	21.5	425 ± 40	1416	1626	1416	1632	109

Table 1 – Radiocarbon dates from the pre AD 1964 earthquake peat layers at Girdwood, Bird Point and Kenai. Dates reported in ^{14}C yr BP and calibrated to 2σ yr AD using IntCal09 (Reimer et al., 2009) in OxCal 4.7 (Bronk Ramsey, 1995). Due to plateaux in the relationship between radiocarbon ages and calendar years from AD 1650 to 1950, calibration of the dates is refined using IntCal09 and the *P_sequence* deposition model in OxCal (Bronk Ramsey, 1995) with k = 500 (Figure 4). The agreement index is a measure of the accuracy of the overall model and individual calibration solution. Bronk-Ramsey (2009) suggests a threshold value of 60% is appropriate. * = those solutions which fall below 60%. The overall performance of each sequence is greater than 60%, giving confidence in the calculated accumulation rates. †Date previously reported in Hamilton and Shennan (2005b).

Graph key		Earth model parameters		
Colour	Model number	Lithospheric thickness (km)	Asthenosphere viscosity (x 10^{19} Pa s)	Mantle viscosity (x 10^{20} Pa s)
	1	110	4.0	4.0
	2	110	0.8	4.0
	3	110	0.4	4.0
	4	110	0.1	4.0
	5	60	4.0	4.0
	6	60	0.8	4.0
	7	60	0.4	4.0
	8	60	0.1	4.0

Table 2 – Key to rheology of Earth models shown in Figure 6. Two models greyed out are those rejected using the GPS data in Figure 6.

EDC component	Inter-seismic (m)	RSL (m)	Co-seismic (m)	Total sedimentation (m)	PMSE change (m)	Time period (AD)	Rate (mm/yr)
Girdwood (GW-2b)							
Whole EDC	1.74	1.40	1.59	1.29	-0.04	1964 - 1100	2.01
First part (silt)	1.24	0.33	1.59	0.87	-0.20	1303 - 1100	6.14
Last part (peat)	0.49	1.07	0.00	0.42	0.16	1964 - 1303	0.74
Bird Point (BP-6)							
Whole EDC	1.72	1.39	1.72	1.25	0.14	1964 - 1100	2.00
First part (silt)	1.41	0.50	1.72	0.87	-0.06	1408 - 1100	4.57
Last part (peat)	0.32	0.90	0.00	0.38	0.20	1964 - 1408	0.57
Ocean View (OV-4)							
Whole EDC	0.76	1.56	0.32	0.79	0.32	1964 - 1100	0.88
First part (silt)	0.60	0.60	0.32	0.35	-0.03	1436 - 1100	1.79
Last part (peat)	0.16	0.95	0.00	0.44	0.35	1964 - 1436	0.30
Kenai (KE-7)							
Whole EDC	not applicable	not applicable	not applicable	not applicable	not applicable	not applicable	not applicable
First part (silt)							
Last part (peat)	0.32	0.44	0.00	0.16	-0.04	1964 - 1509	0.70

Table 3 – Calculation of interseismic rate (final column) using equation 1 (see section 5) over the penultimate earthquake cycle (where applicable) at the four field sites. Palaeo marsh surface elevation (PSME) changes calculated using diatom transfer functions. Calculated rates for last part of EDC cycle (highlighted in blue) used to produce EDC RSL curve in Figure 9C.

Core	Total number of diatom based RSL reconstruction data points	Percentage of RSL data points that overlap with the GIA model predictions of RSL (Figure 9B)	Percentage of RSL data points that overlap with the EDC model predictions of RSL (Figure 9C)	Percentage of RSL data points that overlap with the combined GIA and EDC model predictions of RSL (Figure 9D)
GW-1	10	80 %	20 %	80 %
GW-2b	18	44 %	28 %	89 %
BP-6	20	80 %	40 %	100 %
OV-4	13	100 %	54 %	100 %
KE-7	16	50 %	25 %	100 %
Percentage of total number of RSL data points which overlap with the models of RSL change	not applicable	68.8 %	33.8 %	94.8 %*

Table 4 - A simple assessment as to the degree of fit between the RSL reconstructions and the models of GIA and tectonic RSL change in Figure 9 by calculating the percentage of diatom based RSL reconstruction data points from each core that overlap with one or more of the proposed GIA and EDC models of RSL change. The best fit (*) with the RSL reconstructions are achieved by combining the GIA and tectonic model predictions in Figure 9D. There is still some unexplained misfit which suggests the contribution by some additional Earth process beyond the scope of this paper.

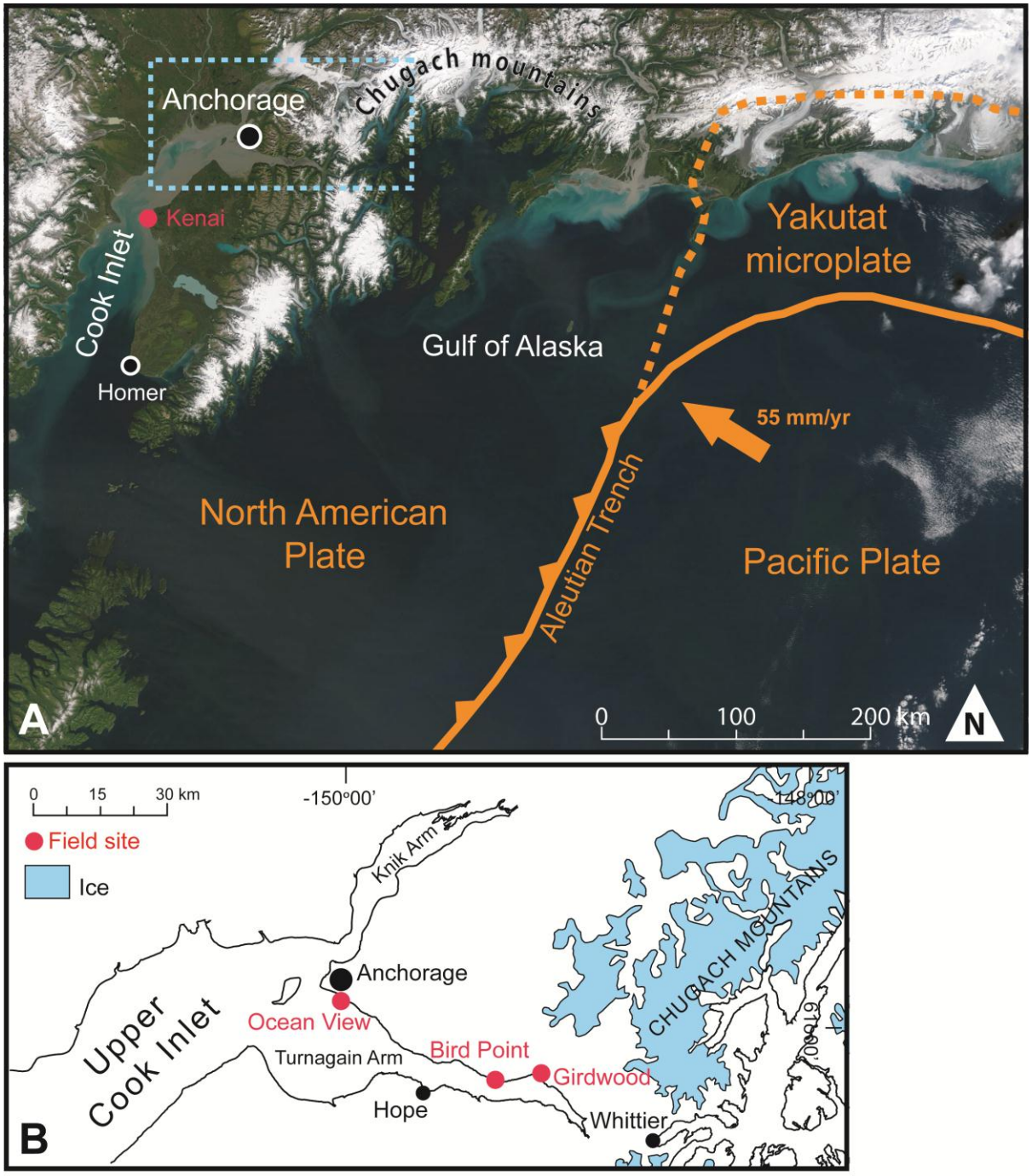

Figure 1: A: Map of south central Alaska showing key tectonic boundaries and main locations mentioned in the text. Satellite image clearly shows regions of mountain glaciers, in particular those in the Chugach Mountains, the centre of LIA ice loading relative to upper Cook Inlet. Larsen et al. (2005) model GIA uplift in south east Alaska, ~850 km east of Anchorage (~350 km to the right of the image). B: Map of Turnagain Arm (dashed box in 'A') showing three tidal marsh field sites and other locations in upper Cook Inlet. Base image in 'A' from NASA MODIS (http://eoimages.gsfc.nasa.gov/ve/4559/Alaska.A2002245.2120.250m.jpg)

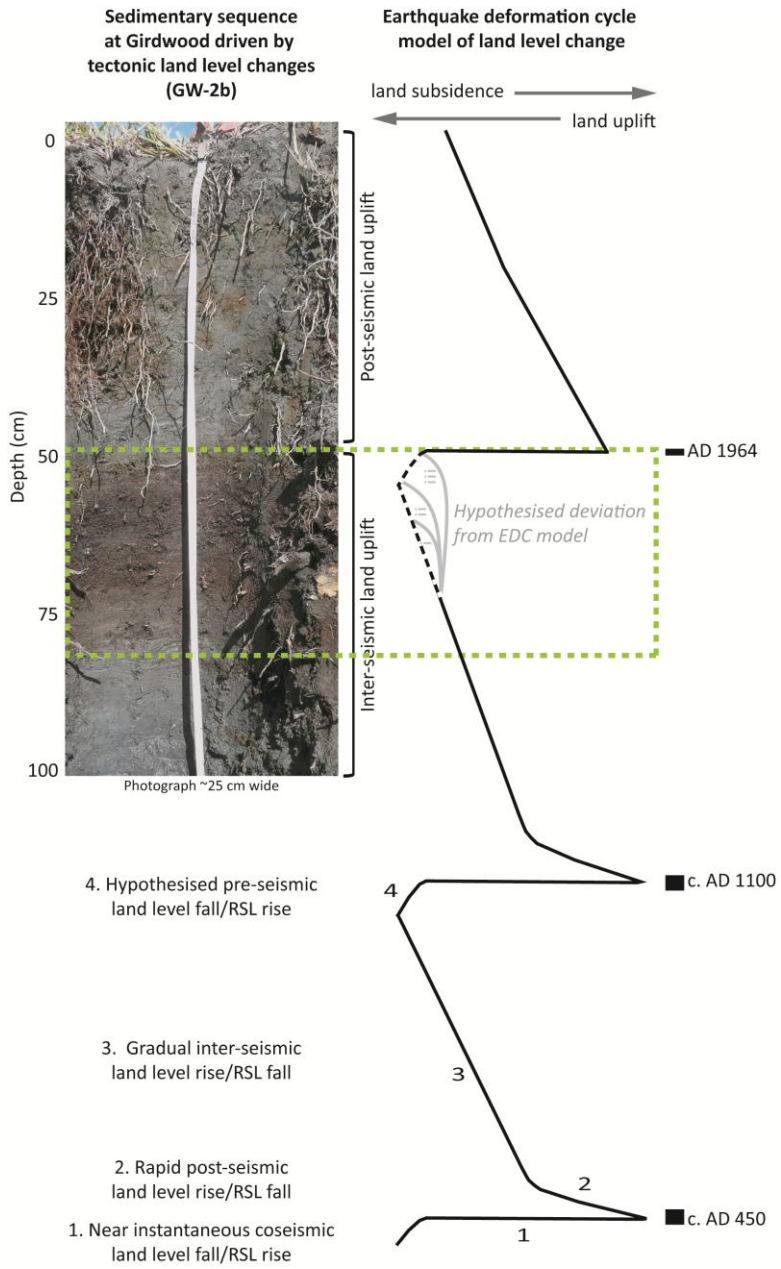

Figure 2: Typical upper Cook Inlet peat-silt couplet and a four phase earthquake deformation cycle (EDC) model (Shennan and Hamilton, 2006) for the last three great earthquakes in south central Alaska: AD 1964, ~ AD 1100 and ~ AD 450. Due to the distance from the subduction trench great earthquakes result in coseismic land subsidence in upper Cook Inlet and rapid RSL rise (1), followed by decades of rapid post-seismic uplift (2) and centuries of gradual interseismic land uplift and RSL fall (3), before a hypothesised period of pre-seismic subsidence (4) in the decades prior to the next great earthquake. This cycle results in a series of sediment sequences where tidal silt becomes more organic grading to peat during the interseismic uplift phase prior to rapid co-seismic submergence and renewed tidal silt accumulation. The EDC framework of tectonically driven land level changes provides a testable model against which to measure non seismic RSL deviations from the tectonic model. This paper focuses on a possible deviation during the penultimate earthquake deformation cycle (illustrated by grey curves) hypothesised by Hamilton and Shennan (2005a) to be due to LIA associated GIA. Non seismic sea-level changes may take a series of forms (i, ii, iii), overprinting the EDC. We focus on the RSL changes reconstructed from the sediments in the region marked by the green box where suitable in-situ material exists to create an adequate age model.

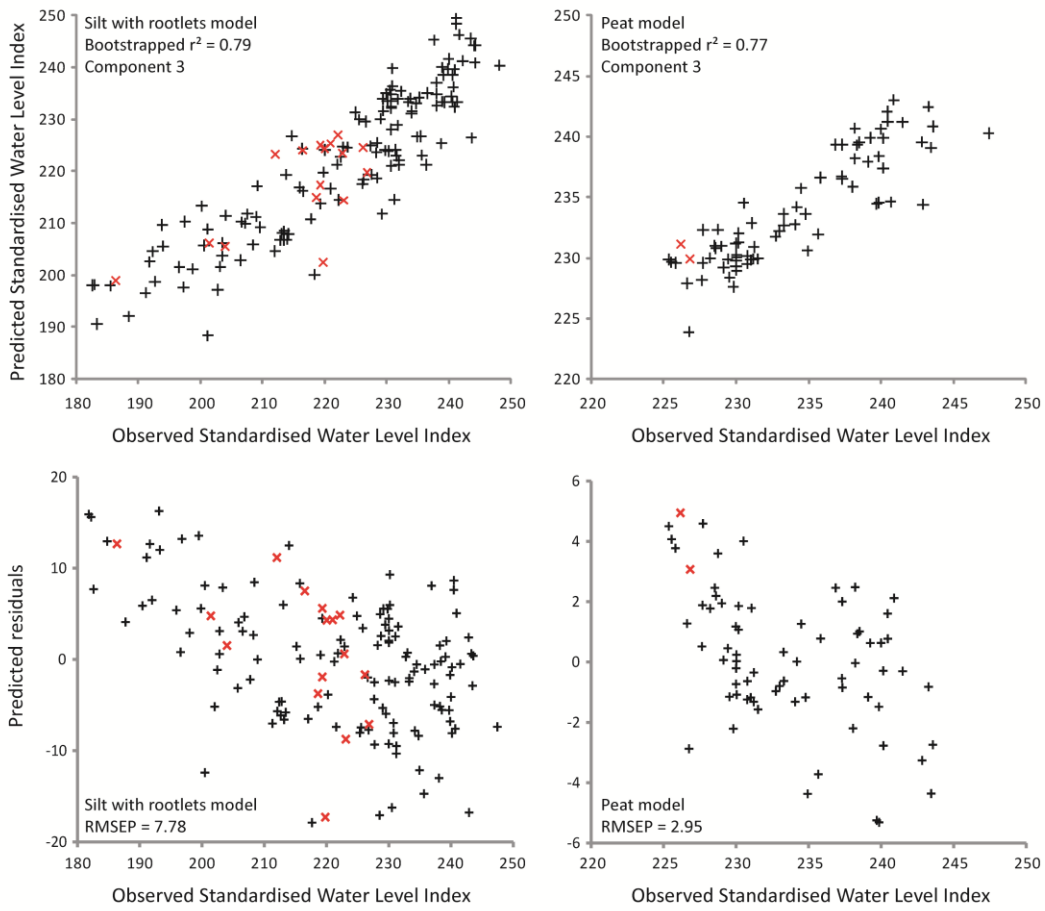

Figure 3 – Upper Cook Inlet transfer function model regression and residuals for the two new restricted sample transfer functions: the silt with rootlets (>3 m MSL/SWLI >180) and the peat (>5 m MSL/SWLI >225) models (see section 3.1 for details). To accommodate for local tidal range differences in upper Cook Inlet we standardise elevations relative to mean higher high water (MHHW) and the difference in elevation between MHHW and MSL, using the standardised water level index (SWLI) equation given in Hamilton and Shennan (2005a), where a SWLI of 200 equals MHHW and a SWLI of 100 equals MSL. Black pluses are samples from the Hamilton and Shennan (2005a) dataset and red crosses are new samples from Hope. The transfer function models use weighted averaging partial least squares component three in C2 (Juggins, 2003) based on selecting the lowest root mean squared error of prediction. There is some structure in the residuals due to other factors beyond elevation controlling modern diatom distribution. However, Hamilton and Shennan (2005a) show elevation is the primary control and the long ecological gradient (>2 standard deviations) allows us to apply unimodal methods of regression.

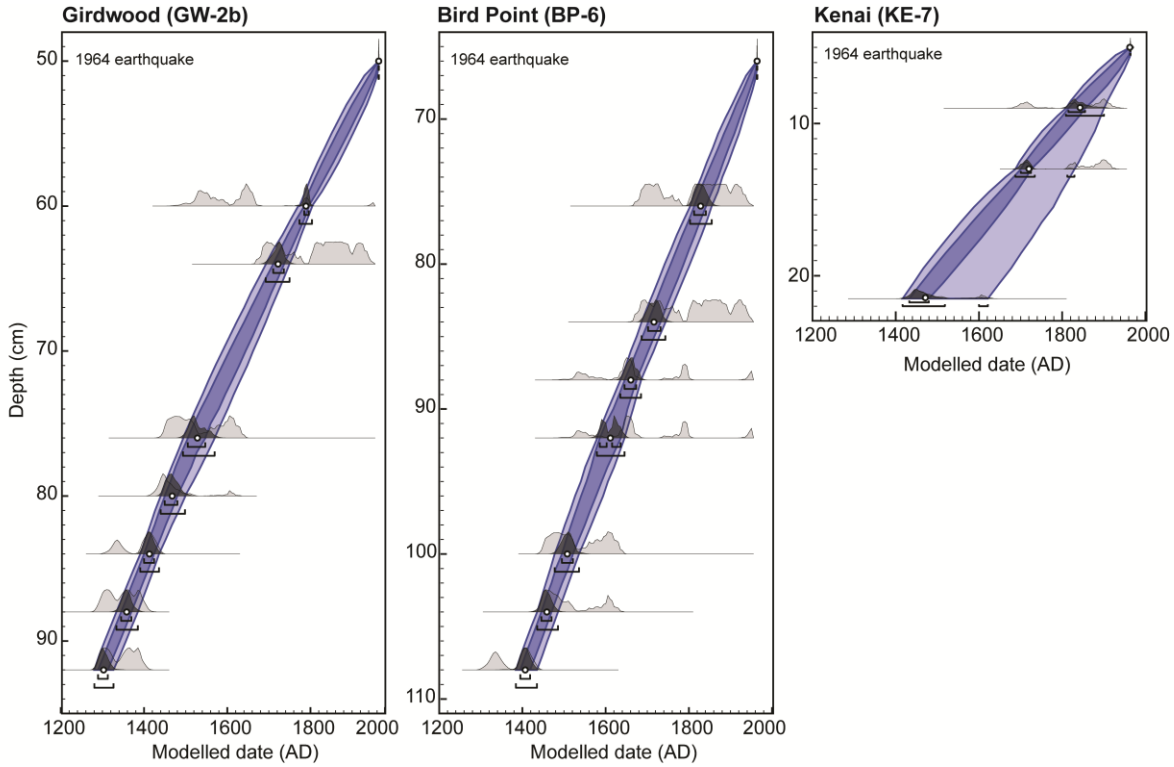

Figure 4 – OxCal depositional age models for Girdwood (GW-2b), Bird Point (BP-6) and Kenai (KE-7) for radiocarbon dates (Table 1) from the upper pre AD 1964 peat layer. All age models use the P_sequence depositional model and IntCal09 calibration curve (Reimer et al., 2009). Plots show IntCal09 likelihood and posterior probability distribution. The blue interpolation envelope shows 2σ (light blue) and 1σ (dark blue) ranges. 2σ fit for KE-7 is poor compared to the other two curves due to the limited number of dates. White circles mark mean calibration solutions which are used to develop the age models in Figure 9.

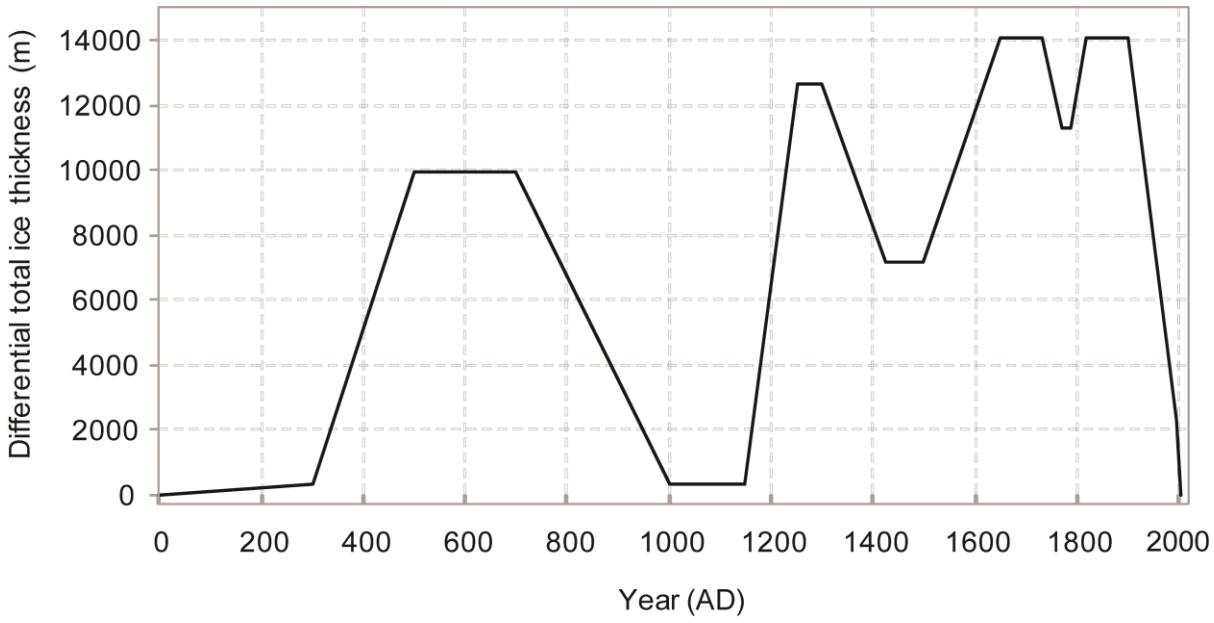

Figure 5 – Ice load history of the Larsen et al. (2005) regional Neoglacial load model shown as differential ice thickness (m) relative to AD 2004. The load is spread over a grid of 531 disks which cover the glaciated regions of Alaska and neighbouring British Columbia. Each disk is 20 km in diameter and has a 20-step time piecewise load history for the past 2000 years (further detail in section 3.3).

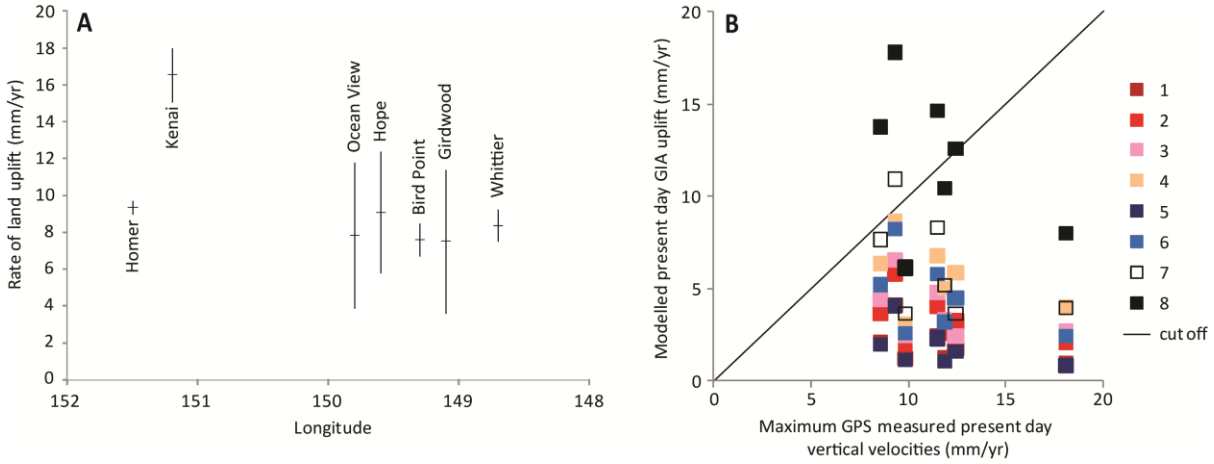

Figure 6 – A: Weighted mean vertical velocities of GPS stations within 10 km of six coastal sites in upper Cook Inlet and Whittier on the western coast of Prince William Sound, (data and uncertainty terms as defined by Freymueller et al. (2008)), relative to the centre of the solid Earth (CE). B: For the seven locations in A, maximum vertical velocities, defined as weighted mean plus uncertainty term, plotted against the TABOO modelled present day GIA uplift for eight Earth models (Table 2). We reject those solutions where the modelled present day GIA exceeds the maximum GPS measured vertical land motion (i.e. above the black 1:1 line).

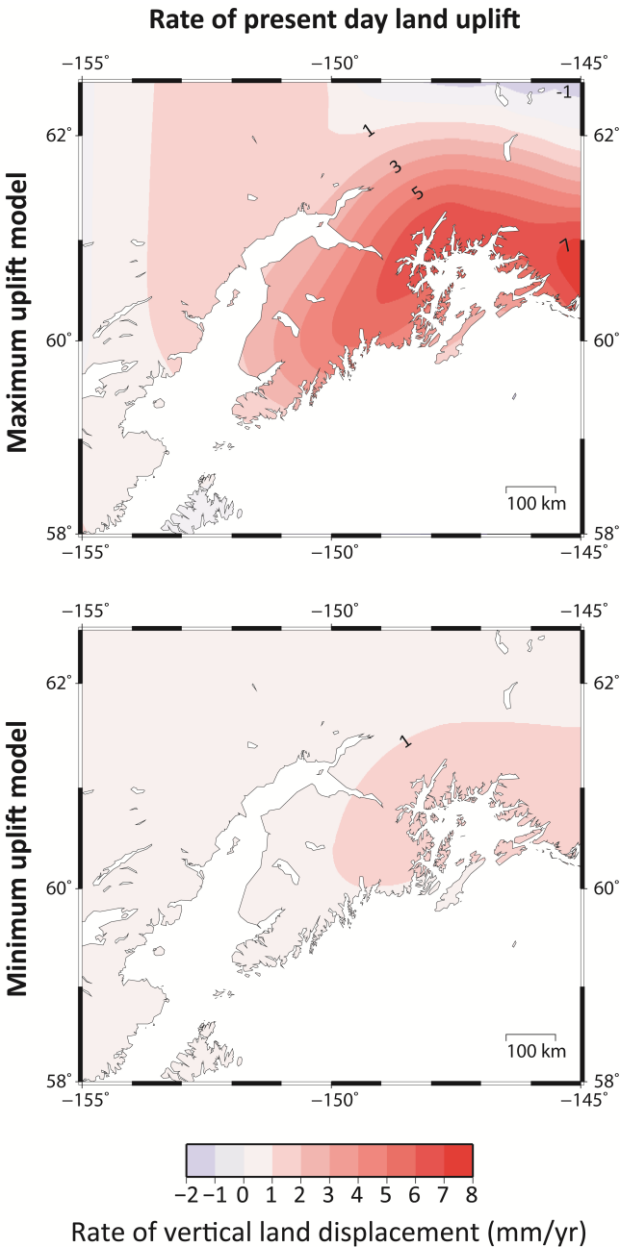

Figure 7 – Spatial representation of maximum (Earth model 4, Table 2) and minimum (Earth model 5, Table 2) modelled rate of present day (AD 2005) land uplift (mm yr^{-1}) in south central Alaska due to LIA GIA. Solid Earth displacement is relative to the centre of solid Earth reference frame. The spatial pattern of radial displacement likely falls within these upper and lower models.

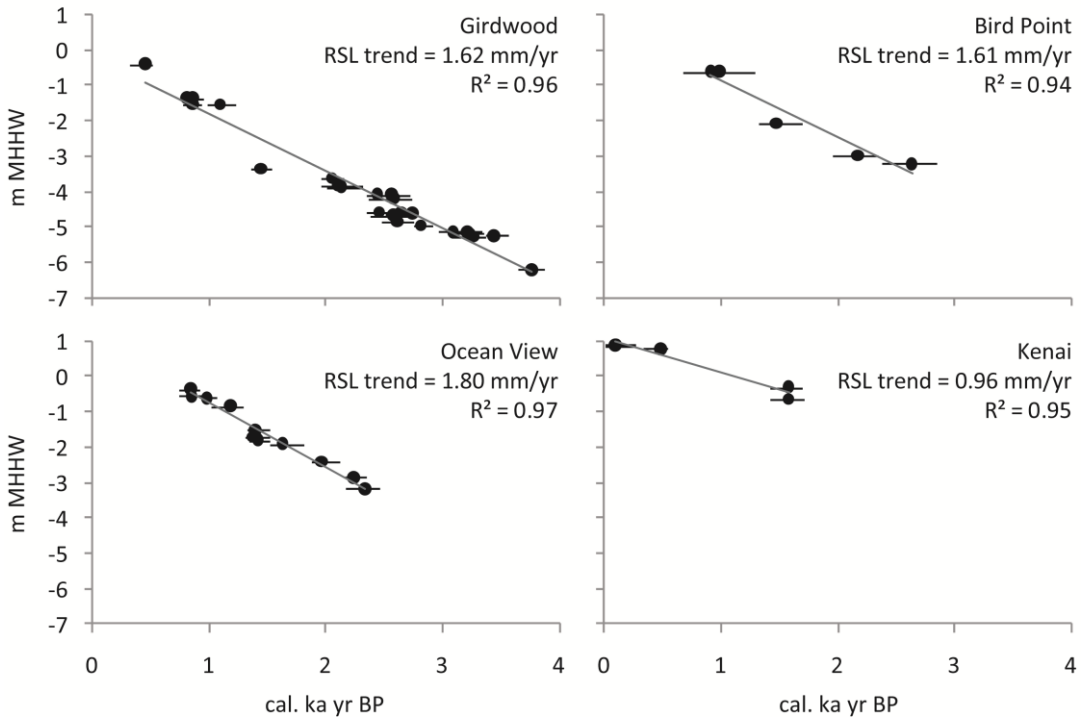

Figure 8 – Late Holocene relative sea-level trends at four sites around upper Cook Inlet. We calculate the rates using published radiocarbon dates (Hamilton and Shennan, 2005b; Hamilton et al., 2005; Shennan and Hamilton, 2006; Shennan et al., 2008; Shennan et al., 2010) alongside new dates in Table 1 from fossil peat layers representing the latter stage of each earthquake cycle (section 3.5), calibrated using IntCal09 (Reimer et al., 2009), which are plotted against the elevation of the radiocarbon sample relative to mean higher high water (m MHHW).

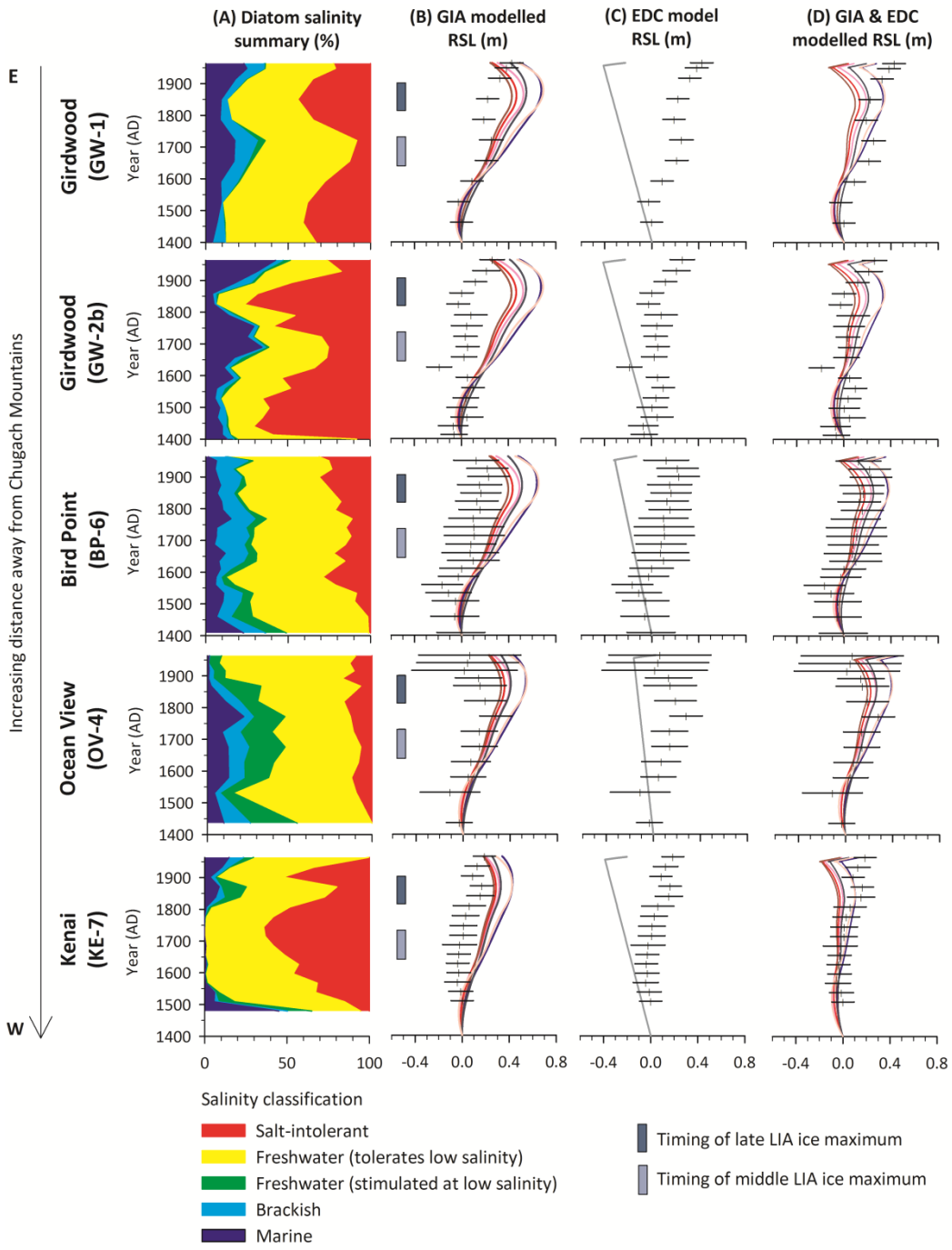

Figure 9 – Integration of geological data and geophysical modelling results with estimates of tectonic land level changes to assess the mechanisms of RSL change. All data plotted against radiocarbon modelled ages (Figure 4 and section 4.3) and standardised as changes relative to AD 1400, or the base of the peat if younger. A: summary of diatom salinities classes for each microfossil sample in the five cores. B: TABOO estimated GIA and geoid deformation driven RSL changes for the six possible Earth models (colours and Earth models as summarised in Table 2), overlain with transfer function based reconstructions of RSL with sample specific error terms. C: EDC model of RSL changes using the interseismic rates calculated in Table 3 and an average 15.5 mm yr^{-1} pre-seismic rate from AD 1952 to AD 1964 (as detailed in section 6.3), overlain by the RSL reconstructions. D: combination of the GIA models in 'B' with the tectonic model in 'C', overlain by the RSL reconstructions. This achieves the best fit between the geological data and model predictions for all five locations.

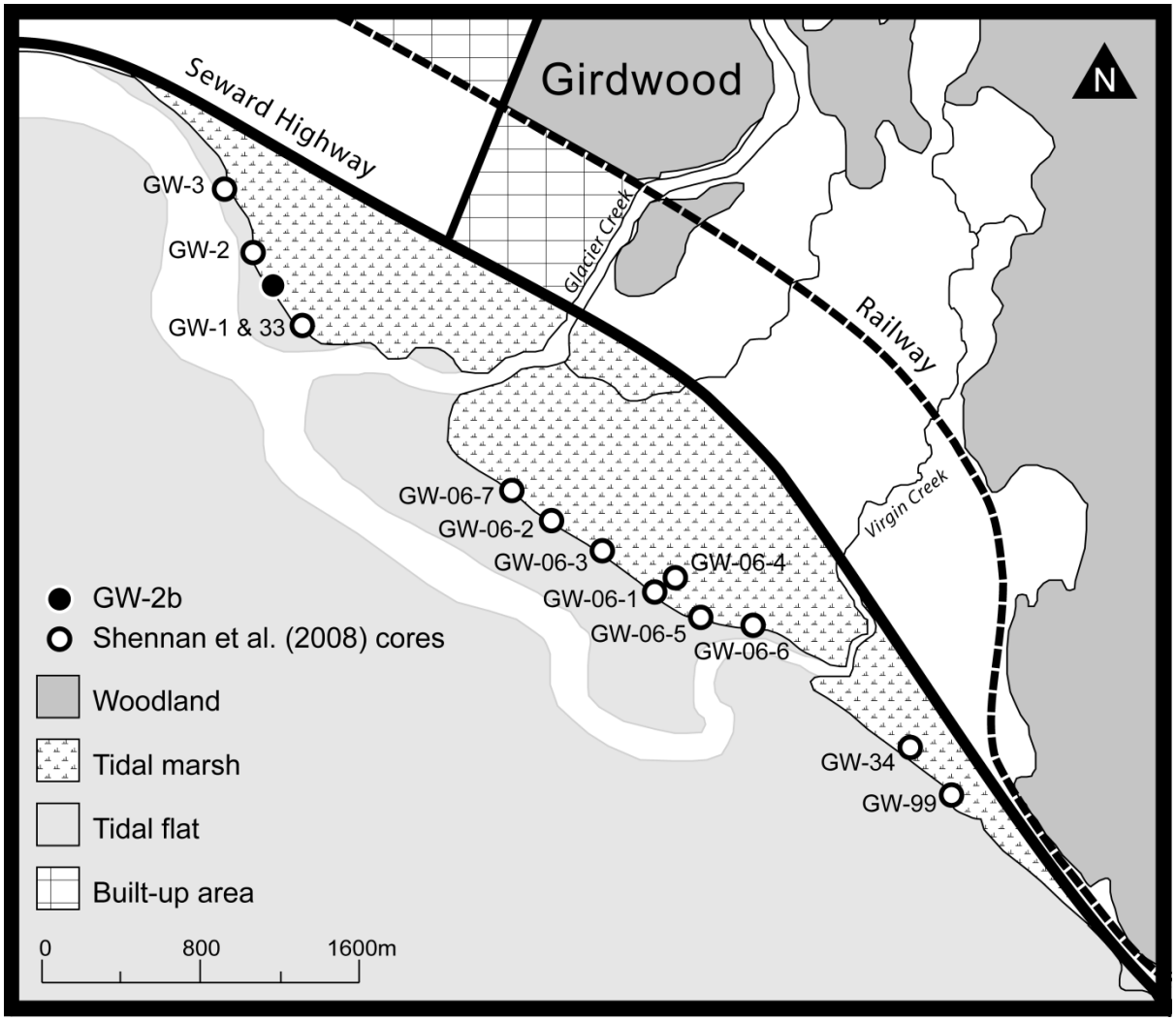

Sup info Figure 1 – Map of Girdwood showing location of GW-2b and other cores summarised in Shennan et al. (2008).

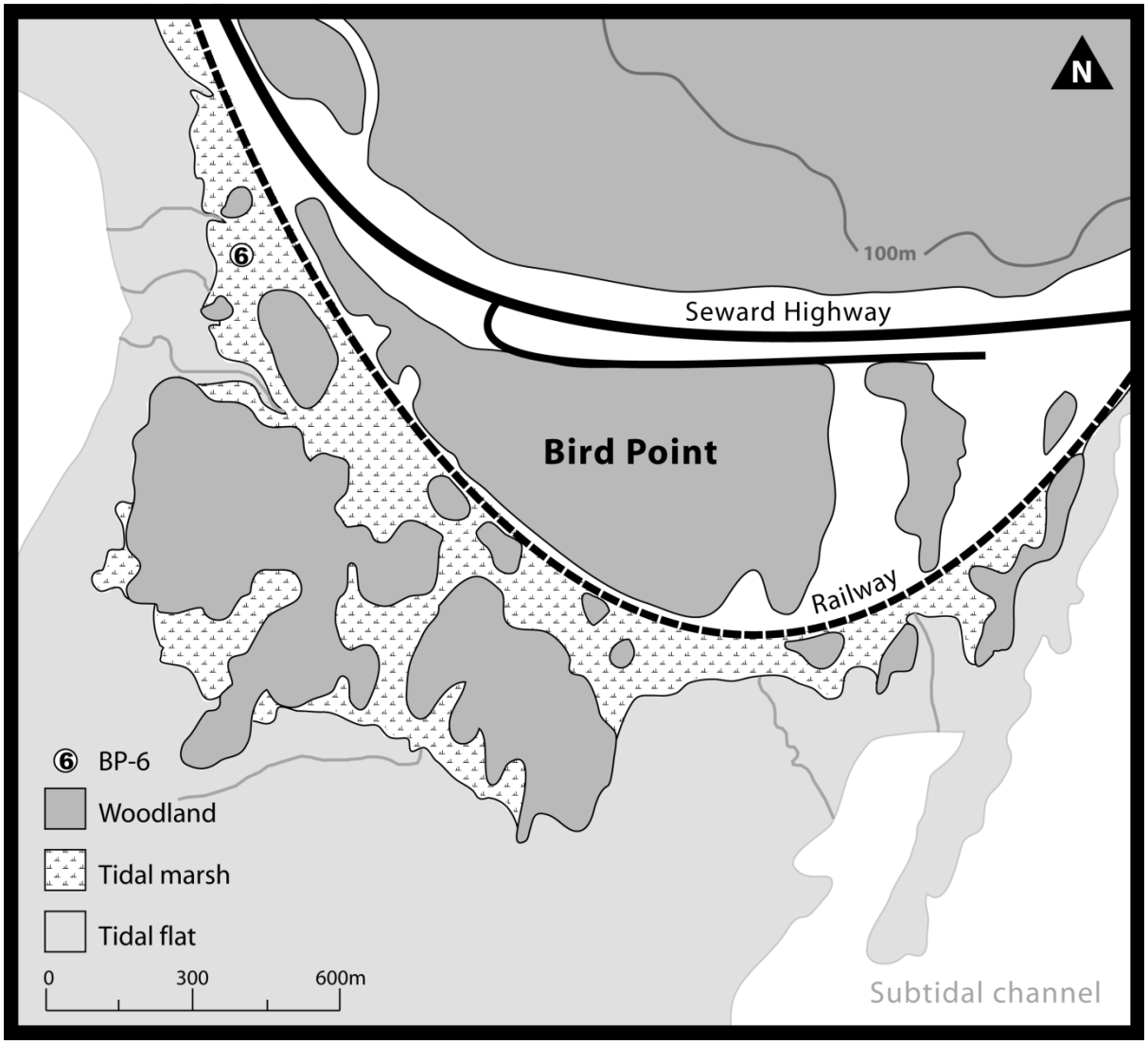

Sup info Figure 2 – Map of Bird Point showing location of BP-6.

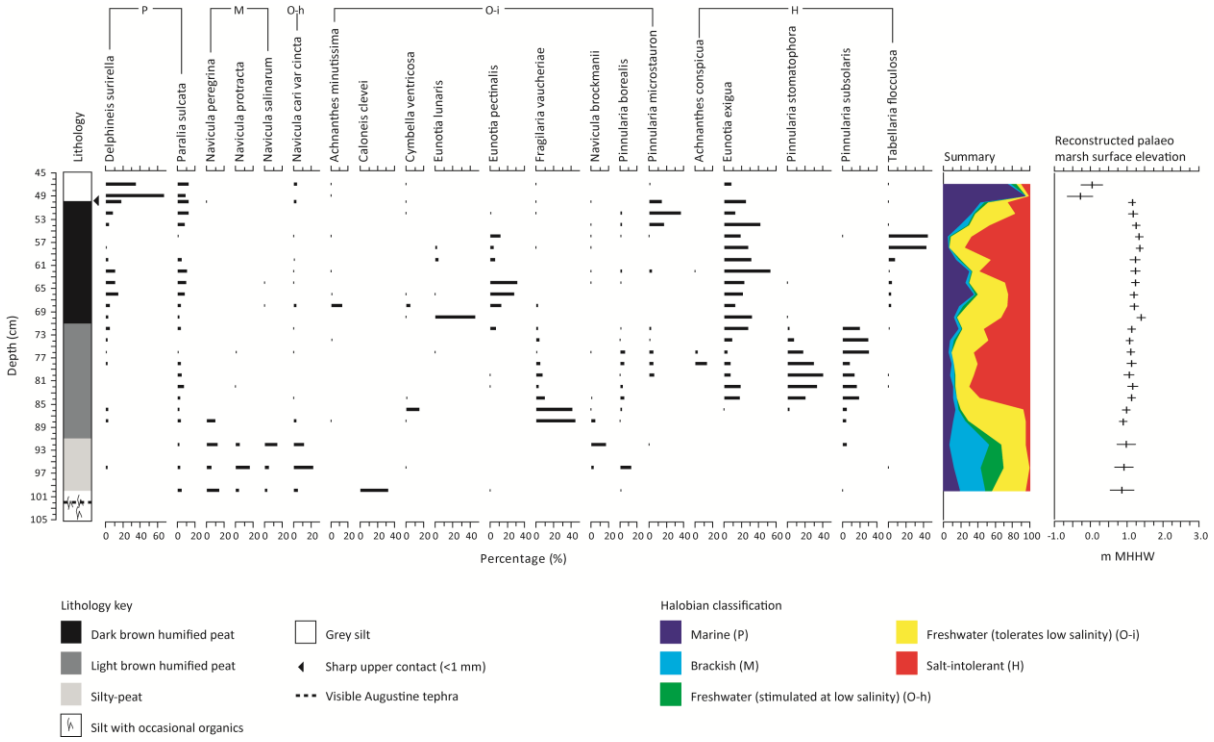

Sup info Figure 3 – Biostratigraphy of GW-2b showing diatoms that account for 10% of total diatom values counted and reconstructions of palaeo marsh surface elevation using the transfer function models as detailed in the main text.

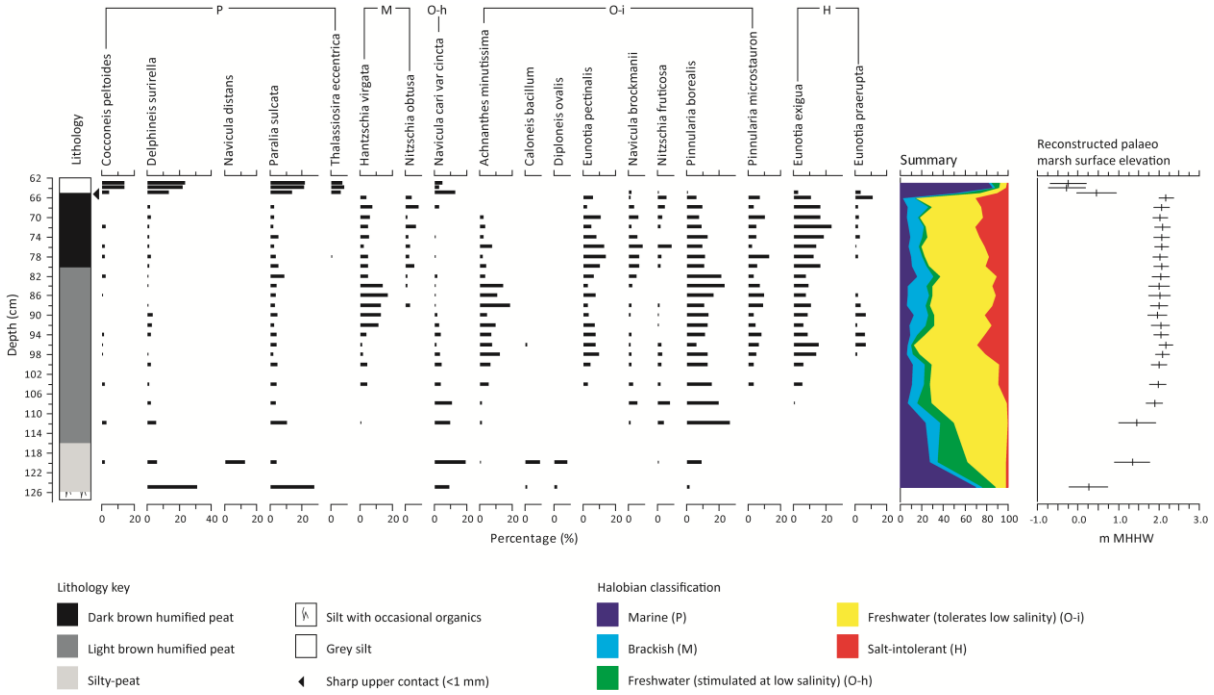

Sup info Figure 4 – Biostratigraphy of BP-6 showing diatoms that account for 7.5% of total diatom values counted reconstructions of palaeo marsh surface elevation using the transfer function models as detailed in the main text.

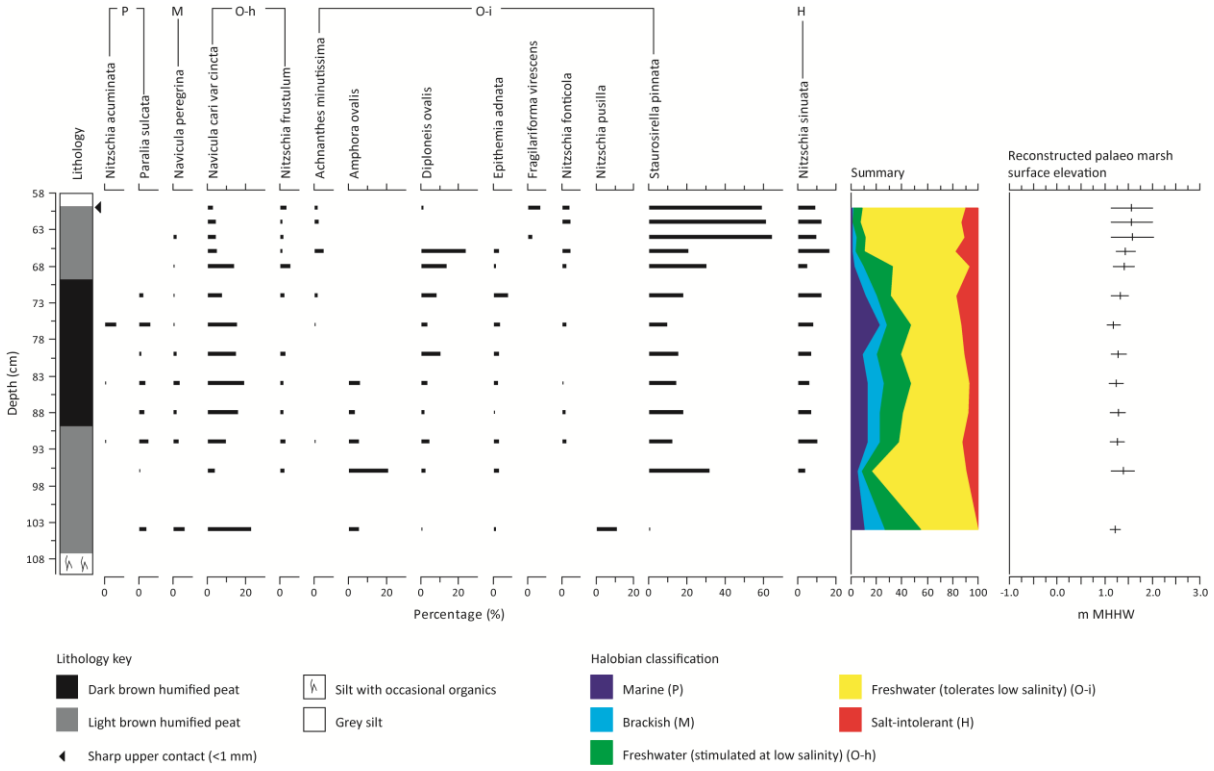

Sup info Figure 5 – Biostratigraphy of OV-4 showing diatoms that account for 5% of total diatom values counted reconstructions of palaeo marsh surface elevation using the transfer function models as detailed in the main text.

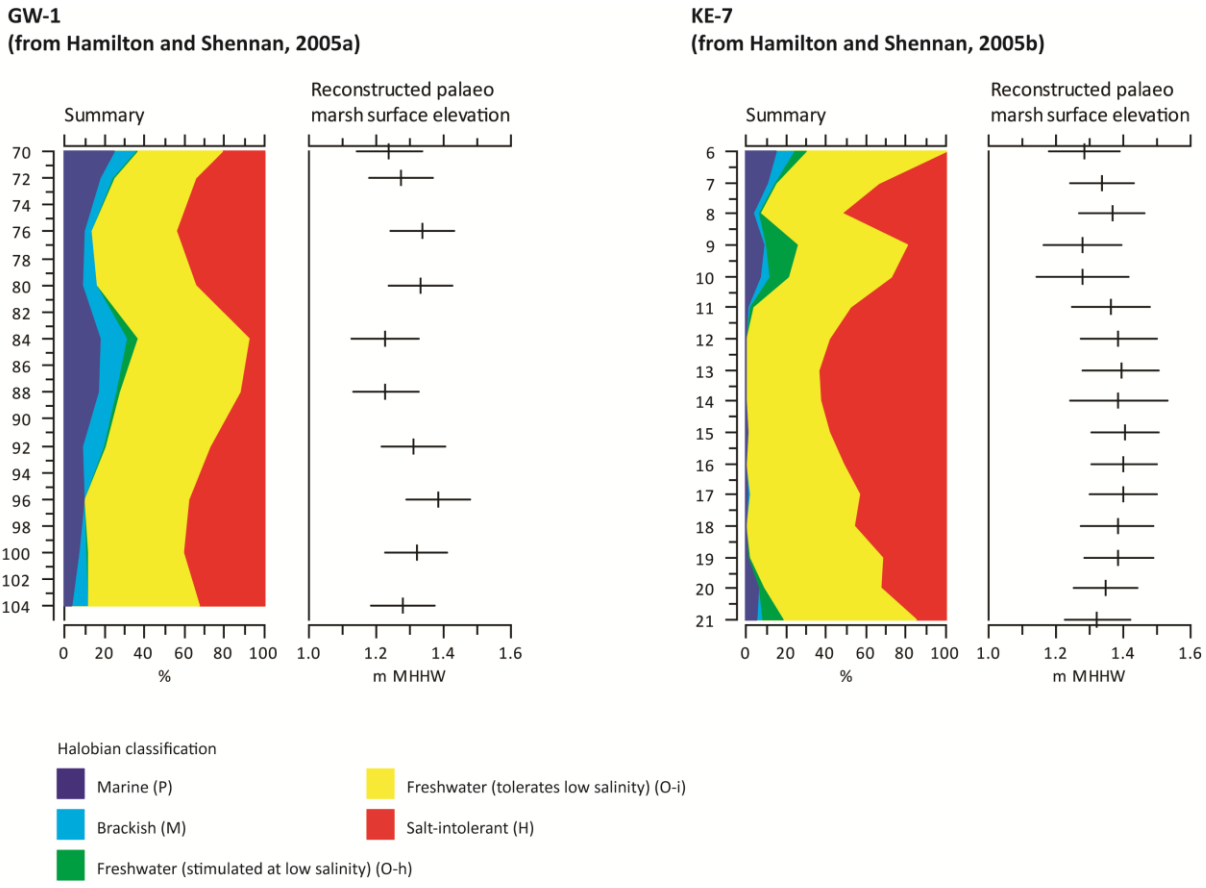

Sup info Figure 6 – Diatom salinity summaries and reconstructions of palaeo marsh surface elevation using the transfer function models as detailed in the main text for GW-1 and KE-7 for those samples shown in Figure 9. The full biostratigraphy for each core is available in Hamilton and Shennan (2005a) and Hamilton and Shennan (2005b) respectively.